

IETI-BASED LOW-RANK METHOD FOR PDE-CONSTRAINED OPTIMIZATION

TOM-CHRISTIAN RIEMER^{*}, ALEXANDRA BÜNGER[†], AND MARTIN STOLL[‡]

Abstract. Isogeometric Analysis (IgA) is a versatile method for the discretization of partial differential equations on complex domains, which arise in various applications of science and engineering. Some complex geometries can be better described as a computational domain by a multi-patch approach, where each patch is determined by a tensor product Non-Uniform Rational Basis Splines (NURBS) parameterization. This allows on the one hand to consider the problem of the complex assembly of mass or stiffness matrices (or tensors) over the whole geometry locally on the individual smaller patches, and on the other hand it is possible to perform local mesh refinements independently on each patch, allowing efficient local refinement in regions of high activity where higher accuracy is required, while coarser meshes can be used elsewhere. Furthermore, the information about differing material models or properties that are to apply in a subdomain of the geometry can be included in the patch in which this subdomain is located. For this it must be ensured that the approximate solution is continuous over the entire computational domain and therefore at the interfaces of two (or more) patches. The most promising approach for this problem, which transfers the idea of Finite Element Tearing and Interconnecting (FETI) methods into the isogeometric setup, was the Isogeometric Tearing and Interconnecting (IETI) method, where by introducing a constraints matrix and associated Lagrange multipliers and formulating it into a dual problem, depending only on the Lagrange multipliers, continuity at the interfaces was ensured in solving the resulting system. In this paper we illustrate that low-rank methods based on the tensor-train format can be generalised for a multi-patch IgA setup, which follows the IETI idea.

Key words. isogeometric analysis, multi-patch, IETI, optimal control, low-rank decompositions, tensor-train format

AMS subject classifications. 65F10, 65F50, 15A69, 93C20

1. Motivation. Isogeometric Analysis (IgA) is a discretization technique used for approximating solutions to a partial differential equation (PDE) defined on a given domain Ω . It was introduced by Hughes, Cottrell and Bazilevs in 2005 [13]. In Isogeometric Analysis the problem domain Ω and the solution space for solving the PDE using a Galerkin approach [34] are parameterized by the same spline functions, typically B-splines or NURBS (Non-Uniform Rational Basis Splines). These basis functions are globally defined and have overlapping supports depending on their degrees. As such these discretizations have a higher computational complexity, increasing exponentially with respect to the dimension of the problem [18], but also allow the relatively easy approximation of domains rather difficult to treat with traditional finite element methods. One of the major research interests in IgA is to find strategies to overcome the complexity drawback and efficiently assemble the system matrices [1, 14, 26, 27].

We here follow the idea of Mantzaflaris et al. [17, 16] of using a low-rank tensor method, which exploits the tensor structure of the basis functions and separates the variables of the integrals. As a result the system matrices are then approximated to high accuracy by a sum of Kronecker products of smaller matrices, which are assembled via univariate integration. We here rely on the method of [5] where the

^{*}Technische Universität Chemnitz, Department of Mathematics, Chair of Scientific Computing, 09107 Chemnitz, Germany, tom-christian.riemer@mathematik.tu-chemnitz.de

[†]University of British Columbia, Computer Science, Vancouver, BC Canada V6T 1Z4, 604 822 3061, alexandra.buenger@mathematik.tu-chemnitz.de

[‡]Technische Universität Chemnitz, Department of Mathematics, Chair of Scientific Computing, 09107 Chemnitz, Germany, martin.stoll@mathematik.tu-chemnitz.de

assembly is carried out using an interpolation step and a low-rank representation of the resulting coefficient tensor. The authors there combine the low-rank method of Mantzaflaris et al. with low-rank tensor-train (TT) calculations [23, 25]. Exploiting the tensor product nature of the arising interpolation, we can calculate a low-rank TT approximation without prior assembly of the full coefficient tensor by means of the Alternating Minimal Energy (AMEn) method [10]. Our goal for this paper is to extend this technique to the case of a multi-patch domain discretized using IgA. This poses the problem that the approximations generated for the corresponding problems can show discontinuities at the interfaces of these patches. We overcome this by transferring the idea of the IETI method from [15] to the low-rank tensor setup. We also want to test our technique on the following problems. We consider the low-rank solution of the elliptic problem defined by Poisson’s equation equipped with homogeneous Dirichlet boundary conditions

$$(1.1) \quad \begin{aligned} -\Delta y &= f && \text{in } \Omega, \\ y &= 0 && \text{on } \partial\Omega. \end{aligned}$$

Here f is some source function and Ω is a given multi-patch geometry parameterized by B-splines or NURBS. The second problem we consider is an optimization problem where the heat equation becomes the constraint of an objective function that we want to minimize, i.e.,

$$(1.2) \quad \min_{y,u} \quad \frac{1}{2} \int_0^T \int_{\Omega} (y-\hat{y})^2 \, dx \, dt + \frac{\alpha}{2} \int_0^T \int_{\Omega} u^2 \, dx \, dt$$

$$(1.3) \quad \text{s.t.} \quad y_t - \Delta y = u \quad \text{in } (0, T) \times \Omega,$$

$$(1.4) \quad y = 0 \quad \text{on } (0, T) \times \partial\Omega,$$

$$(1.5) \quad y = y_0 \quad \text{on } \Omega \text{ for } t = 0,$$

with a desired state \hat{y} and control u on a multi-patch geometry Ω . The discretization of (1.2) to (1.5) in this paper will be performed by IgA. Tensor techniques for IgA have shown promising results in many areas and we refer to [19] for the single-patch case and for the multi-patch case to [20]. In the latter the authors use Tucker tensors for the low-rank approximation and focus on the forward elasticity simulation on conforming (or fully matching) multi-patch geometries. In this paper we focus on the approximation via the tensor-train format and provide approaches for the solution of the optimal control problem, also on nonconforming geometries. Nevertheless, their method and ours are similar in spirit by aiming at breaking the curse of dimensionality by relying on low-rank tensor formats.

The paper is structured as follows: In the preliminaries we first discuss low-rank tensor formats in subsection 2.1, in subsection 2.2 we introduce the basics of IgA and discuss how the tensor-train format can be used so that the system matrices or tensors can be assembled low-rank, in subsection 2.3 we present our multi-patch IgA notation and state the general problem. In section 3, we present how the idea of the IETI method [15] can be generalised for the tensor setup and how the so-called jump tensors can be defined. Then we explain in section 4 how the resulting low-rank IETI method works to generate continuous low-rank approximations over multi-patch geometries. In section 5, we show how this method can be used to find an approximation of the optimization problem described by (1.2) to (1.5). The results of our numerical experiments are presented in section 6. In section 7, we summarise the insights and results, concluding our work.

2. Preliminaries.

2.1. Low-rank tensor format. The most well-known technique for low-rank approximations is the singular value decomposition, illustrated for a matrix $W \in \mathbb{R}^{n_1 \times n_2}$ as

$$(2.1) \quad W = U \Sigma V^\top \approx \sum_{r=1}^R u_r \sigma_r v_r^\top = \sum_{r=1}^R (u_r \sqrt{\sigma_r}) \otimes (v_r \sqrt{\sigma_r}).$$

with $U \in \mathbb{R}^{n_1 \times n_1}$, $V \in \mathbb{R}^{n_2 \times n_2}$ with their columns denoted by u_r and v_r , and $\Sigma \in \mathbb{R}^{n_1 \times n_2}$ is the rectangular matrix holding the sorted singular values σ_i , $i = 1, \dots, \min(n_1, n_2)$ on its main diagonal. The best low-rank approximation is obtained by the truncated SVD where we truncate all singular values below some given threshold resulting in a rank- R approximation, where R is the number of used singular values and therefore the number of summands in (2.1).

In the high-dimensional case we need low-rank tensor approximation of a D -dimensional tensor. Such approximations are given by, e.g., the higher-order singular value decomposition (HOSVD) [6], or a canonical polyadic decomposition (CP) [31]. However, the approximation problem in the CP format is typically ill-posed [7] and might be numerically unstable. The HOSVD (known also as the Tucker format) still contains the curse of dimensionality as it relies on the dimension of the original tensor. We switch to the more robust tensor-train (TT) decomposition [23] in this paper also given the availability of appropriate methods within a robust software framework.

A tensor $W \in \mathbb{R}^{n_1 \times \dots \times n_D}$ is given in the TT format if it is written as

$$(2.2) \quad W(i_1, \dots, i_D) = W^{(1)}(i_1) \cdots W^{(D)}(i_D),$$

where $W^{(d)}(\cdot) \in \mathbb{R}^{R_{d-1} \times n_d \times R_d}$ are the TT cores, which can be understood as parameter dependent matrices $W^{(d)}(i_d)$, $i_d = 1, \dots, n_d$, of size $R_{d-1} \times R_d$ with $R_0 = R_D = 1$ [23]. The TT format can be rewritten into a canonical representation as

$$(2.3) \quad W = \sum_{r_1=1}^{R_1} \cdots \sum_{r_D=1}^{R_D} \bigotimes_{d=1}^D W^{(d)}(r_{d-1}, :, r_d).$$

2.2. Low-rank IgA. Isogeometric analysis allows to represent a geometry exactly using a set of B-splines or NURBS [30] and by using the same basis functions for the solution space of a PDE on this geometry lies at the heart of the IgA method and its success in scientific computing [13, 21]. We here briefly review some important properties of the method with a focus on deriving the discretized equations.

A set of n B-splines is uniquely defined by its degree $p \in \mathbb{N}_0$ and the knot vector $\xi = \{\xi_1, \dots, \xi_{n+p+1}\}$ with

$$(2.4) \quad 0 = \xi_1 = \cdots = \xi_{p+1} < \xi_{p+2} \leq \cdots \leq \xi_n < \xi_{n+1} = \cdots = \xi_{n+p+1} = 1,$$

where the end knots appear $p+1$ times and for all other knots, duplicate appearances are allowed up to multiplicity p . Here $n \in \mathbb{N}$ denotes the number of B-splines $\beta_{i,p}$, with $i = 1, \dots, n$.

For each knot vector ξ as in (2.4), the according B-splines $\beta_{i,p}$ of degree p , with $i = 1, \dots, n$, are uniquely defined by a recursion formula. The resulting B-splines $\beta_{i,p}$ have the local support $[\xi_i, \xi_{i+p+1}]$. We use \mathbb{S}_ξ^p to denote the spline space spanned by the B-splines with degree p and knot vector ξ and we refer to the basis functions as

$\beta_i \in \mathbb{S}_\xi^p$. In order to increase the accuracy of the numerical approximation a refinement strategy based on knot insertion is often applied and we refer to [13, 30].

For D -dimensional geometries we use tensor products of univariate spline spaces considering D different univariate spline spaces $\mathbb{S}_{\xi_d}^{p_d}$, where one can assume that each space has the degree p_d and an individual knot vector ξ_d , with $d = 1, \dots, D$. Here, $\hat{x}^{(d)} \in [0, 1]$ are the $1D$ variables and $\beta_{1_d}^{(d)}, \dots, \beta_{n_d}^{(d)}$ the basis functions. The resulting spline space is then denoted by $\mathbb{S}_D = \mathbb{S}_{\xi_1}^{p_1} \otimes \dots \otimes \mathbb{S}_{\xi_D}^{p_D}$. For simplicity we assume further that $p_d = p \forall d$ and the index p_d will be omitted from $\mathbb{S}_{\xi_d}^p$ in the remainder due to better readability. The basis functions of \mathbb{S}_D are denoted by

$$\beta_{\mathbf{i}}(\hat{x}) = \prod_{d=1}^D \beta_{i_d}^{(d)}(\hat{x}^{(d)}),$$

with multi-index $\mathbf{i} \in \mathbf{I} = \{(i_1, \dots, i_D) : i_d \in \{1, \dots, n_d\}, d = 1, \dots, D\}$ and variables $\hat{x} = [\hat{x}^{(1)}, \dots, \hat{x}^{(D)}]^\top \in [0, 1]^D$. All multivariate basis functions evaluated at a point $\hat{x} \in [0, 1]^D$ can be written as a tensor product

$$B(\hat{x}) = \bigotimes_{d=1}^D B^{(d)}(\hat{x}^{(d)}) \in \mathbb{R}^{n_1 \times \dots \times n_D},$$

where $B^{(d)}(\hat{x}^{(d)}) = [\beta_{1_d}^{(d)}(\hat{x}^{(d)}), \dots, \beta_{n_d}^{(d)}(\hat{x}^{(d)})]^\top \in \mathbb{R}^{n_d}$ is a vector holding the univariate B-splines in dimension $d = 1, \dots, D$.

To use these functions for solving a PDE on the domain $\Omega \subset \mathbb{R}^D$ we need a B-spline geometry mapping $G: \hat{\Omega} \rightarrow \Omega$ from the D -dimensional unit cube $\hat{\Omega} := [0, 1]^D$ onto Ω . This is given by

$$(2.5) \quad G(\hat{x}) = \sum_{\mathbf{i} \in \mathbf{I}} C_{\mathbf{i}} \beta_{\mathbf{i}}(\hat{x}) = C : B(\hat{x}),$$

where $C_{\mathbf{i}} \in \mathbb{R}^D$ are the control points. All control points and evaluations of the B-splines are organised in the tensors $C \in \mathbb{R}^{D \times n_1 \times \dots \times n_D}$ and $B(\hat{x}) \in \mathbb{R}^{n_1 \times \dots \times n_D}$, respectively. Here, $:$ denotes the Frobenius product. To overcome some limitations of the B-spline approach NURBS (Non-uniform rational B-splines) have been used [29] quite extensively but will not be discussed further here.

The discretization of the PDE is usually obtained from a weak formulation where we compute approximations of $y \in H_0^1(\Omega)$ with discrete functions $y_h \in V_h \subset H_0^1(\Omega)$ using B-splines. In IgA, the same splines that are used in the construction of the geometry mapping (2.5) are used to parameterize the solution space, i.e. $V_h = \text{span} \left\{ \hat{\beta}_{\mathbf{i}} := \beta_{\mathbf{i}} \circ G^{-1} : \mathbf{i} \in \mathbf{I}_0 \right\} \subset H_0^1(\Omega)$ with basis functions $\beta_{\mathbf{i}} \in \mathbb{S}_D$ and an index set $\mathbf{I}_0 = \{(i_1, \dots, i_D) : i_d \in \{2, \dots, n_d - 1\}, d = 1, \dots, D\} \subset \mathbf{I}$ in which the first and last index of \mathbf{I} in each dimension are omitted, since the remaining splines with index in $\mathbf{I} \setminus \mathbf{I}_0$ are zero for homogeneous Dirichlet conditions. To improve readability, we make an index shift so that $\mathbf{I}_0 = \{(i_1, \dots, i_D) : i_d \in \{1, \dots, \tilde{n}_d\}, d = 1, \dots, D\}$. The functions $y_h \in V_h$ are linear combinations of the basis functions $y_h = \sum_{\mathbf{i} \in \mathbf{I}_0} y_{\mathbf{i}} (\beta_{\mathbf{i}} \circ G^{-1})$ with coefficients $y_{\mathbf{i}} \in \mathbb{R}$. The tensor product structure of \mathbb{S}_D induces a tensor product structure of the solution space V_h , since each basis function $\hat{\beta}_{\mathbf{i}} \in V_h$, $\mathbf{i} = (i_1, \dots, i_D) \in \mathbf{I}_0$, can be represented as

$$(2.6) \quad \hat{\beta}_{\mathbf{i}}(x) = \beta_{\mathbf{i}}(G^{-1}(x)) = \beta_{i_1}^{(1)}(G^{-1}(x)^{(1)}) \cdots \beta_{i_D}^{(D)}(G^{-1}(x)^{(D)}),$$

where $G^{-1}(x)^{(d)} \in [0, 1]$ is the d -th component of the inverse of the geometry mapping and the $\beta_{i_d}^{(d)} \in \mathbb{S}_{\xi_d}$, $d = 1, \dots, D$, are the univariate splines.

The space V_h is now used for the Galerkin discretization, resulting in the discrete mass and stiffness terms

$$a_m(u_h, v_h) = \int_{\Omega} u_h(x) v_h(x) dx = \int_{\hat{\Omega}} \sum_{i \in \mathbf{I}_0} u_i \beta_i(\hat{x}) \sum_{j \in \mathbf{I}_0} v_j \beta_j(\hat{x}) \omega(\hat{x}) d\hat{x},$$

$$a_s(u_h, v_h) = \int_{\Omega} \nabla u_h(x) \cdot \nabla v_h(x) dx = \int_{\hat{\Omega}} \left(Q(\hat{x}) \sum_{i \in \mathbf{I}_0} u_i \nabla \beta_i(\hat{x}) \right) \cdot \sum_{j \in \mathbf{I}_0} v_j \nabla \beta_j(\hat{x}) d\hat{x},$$

for $u_h, v_h \in V_h$, with the additional terms stemming from the domain transformation,

$$\omega(\hat{x}) = |\det \nabla G(\hat{x})| \quad \in \mathbb{R},$$

$$Q(\hat{x}) = \left(\nabla G(\hat{x})^T \nabla G(\hat{x}) \right)^{-1} |\det \nabla G(\hat{x})| \quad \in \mathbb{R}^{D \times D},$$

as introduced in [17]. The corresponding mass and stiffness terms can be written in tensor form, i.e., the mass tensor

$$(2.7) \quad M = \int_{\hat{\Omega}} \omega(\hat{x}) B(\hat{x}) \otimes B(\hat{x}) d\hat{x} \quad \in \mathbb{R}^{(\tilde{n}_1, \dots, \tilde{n}_D) \times (\tilde{n}_1, \dots, \tilde{n}_D)}.$$

Similarly, we can write the stiffness tensor as

$$(2.8) \quad K = \int_{\hat{\Omega}} [Q(\hat{x}) \cdot (\nabla \otimes B(\hat{x}))] \cdot (\nabla \otimes B(\hat{x})) d\hat{x} \quad \in \mathbb{R}^{(\tilde{n}_1, \dots, \tilde{n}_D) \times (\tilde{n}_1, \dots, \tilde{n}_D)}.$$

The computation and storage of (2.7) and (2.8) can be extremely expensive due to multi-dimensional quadrature and the overlapping support of B-splines with high degrees. But it has been observed that these tensors can be well approximated in low-rank tensor formats [17, 5] based on a low-rank approximation of the coupling terms in the integral. For that we approximate the arising multi-dimensional integrals as products of univariate integrals. The ingredients for the mass and stiffness tensors are all univariately defined, except for the weight functions $\omega(\hat{x})$ and $Q(\hat{x})$, which are determined by the geometry mapping (2.5) but are not separable into one-dimensional factors. We therefore interpolate these weight functions by a combination of univariate B-splines of higher order $\hat{B}(\hat{x}) \in \mathbb{R}^{(\hat{n}_1, \dots, \hat{n}_D)}$, i.e.

$$(2.9) \quad \omega(\hat{x}) \approx W : \hat{B}(\hat{x}).$$

For that we follow the approach introduced in [5] by computing a low-rank approximation in TT format (2.3) of the coefficient tensor $W \in \mathbb{R}^{(\hat{n}_1, \dots, \hat{n}_D)}$

$$W_R := \sum_{r_1=1}^{R_1} \cdots \sum_{r_D=1}^{R_D} \bigotimes_{d=1}^D W_R^{(d)}(r_{d-1}, :, r_d) = \sum_{r=1}^R \bigotimes_{d=1}^D w_r^{(d)} \approx W,$$

where $w_r^{(d)} \in \mathbb{R}^{\hat{n}_d}$ and $R = R_1 \cdots R_D$. With this we get a low-rank representation of the weight function,

$$\omega(\hat{x}) \approx W_R : \hat{B}(\hat{x}) = \sum_{r=1}^R \prod_{d=1}^D w_r^{(d)} \cdot \hat{B}^{(d)}(\hat{x}^{(d)}),$$

where $\hat{B}^{(d)}(\hat{x}^{(d)}) \in \mathbb{R}^{\hat{n}_d}$ denotes the vector holding all univariate basis functions evaluated in $\hat{x}^{(d)} \in [0, 1]$. As a result the integrands are separable and we can write the mass tensor (2.7) as a sum of tensor products of small univariate mass matrices

$$(2.10) \quad \begin{aligned} M &= \sum_{r=1}^R \bigotimes_{d=1}^D \int_0^1 \left(w_r^{(d)} \cdot \hat{B}^{(d)}(\hat{x}^{(d)}) \right) B^{(d)}(\hat{x}^{(d)}) \otimes B^{(d)}(\hat{x}^{(d)}) \, d\hat{x}^{(d)} \\ &= \sum_{r=1}^R \bigotimes_{d=1}^D M_r^{(d)}. \end{aligned}$$

The same procedure can be applied to each entry of $Q(\hat{x})$ such that we get a low-rank tensor representation of (2.8) as

$$(2.11) \quad K = \sum_{k,l=1}^D \sum_{r=1}^R \bigotimes_{d=1}^D K_{k,l,r}^{(d)}.$$

We refer to [5] for details and to the codes on our website [4].

2.3. Multi-patch IgA. In a multi-patch setting we assume that the geometric shape $\Omega \subset \mathbb{R}^D$ can be decomposed into N_P many single-patch NURBS parameterizations, such as (2.5), i.e.

$$G^{(j)}(\hat{\Omega}) = \Omega^{(j)} \subset \Omega, \quad j = 1, \dots, N_P,$$

such that

$$\bar{\Omega} = \bigcup_{j=1}^{N_P} \bar{\Omega}^{(j)} \quad \text{and} \quad \Omega^{(j)} \cap \Omega^{(k)} = \emptyset.$$

We note that the parameter space $\hat{\Omega} := [0, 1]^D$ is the same for each parameterization $G^{(j)}$. The multi-patch geometries considered in this paper are all 3-dimensional, so from now on we set $D = 3$ to simplify the notation. Further we assign all variables belonging to the patch $\Omega^{(j)}$, such as basis functions, control points, index sets, etc. a superscript (j) .

As in the single-patch case, the same splines to represent the geometry Ω are used to approximate the solution of the underlying PDE problem. Since each patch $\Omega^{(j)}$ has its own tensor product spline space $\mathbb{S}_3^{(j)} = \mathbb{S}_{\xi_1}^{(j)} \otimes \mathbb{S}_{\xi_2}^{(j)} \otimes \mathbb{S}_{\xi_3}^{(j)}$ with parameterization $G^{(j)}: \hat{\Omega} \rightarrow \Omega^{(j)}$, we define a local solution space for each patch via

$$V_h^{(j)} = \text{span} \left\{ \hat{\beta}_{\mathbf{i}}^{(j)} := \beta_{\mathbf{i}}^{(j)} \circ G^{(j)-1} : \mathbf{i} \in \mathbf{I}_0^{(j)} \right\} \subset H^1(\Omega^{(j)}),$$

where $\mathbf{I}_0^{(j)} \subset \mathbf{I}^{(j)}$ contains the indices of all splines of patch $\Omega^{(j)}$ whose support does not lie on $\partial\Omega \cap \partial\Omega^{(j)}$. As in the single-patch case, the splines of the remaining indices can be considered as zero. We assume that this set of indices has a tensor structure, i.e. $\mathbf{I}_0^{(j)} = \left\{ (i_1^{(j)}, i_2^{(j)}, i_3^{(j)}) : i_d^{(j)} \in \{1, \dots, \tilde{n}_d^{(j)}\}, d = 1, 2, 3 \right\} \subset \mathbb{N}^{\tilde{n}_1^{(j)} \times \tilde{n}_2^{(j)} \times \tilde{n}_3^{(j)}}$. We note that the solution space $V_h^{(j)}$, $j = 1, \dots, N_P$, has a tensor product structure induced by $\mathbb{S}_3^{(j)}$, since all basis functions can be written as in (2.6).

The space of functions on Ω which are locally in $V_h^{(j)}$ is denoted by

$$\Pi V_h = \left\{ y \in \mathcal{L}^2(\Omega) : y|_{\Omega^{(j)}} \in V_h^{(j)}, \forall j = 1, \dots, N_P \right\}.$$

Each function $y_h \in \Pi V_h$, $y_h : \Omega \rightarrow \mathbb{R}$, can be represented patch-wise by a linear combination of the basis functions of the corresponding patch $V_h^{(j)}$ with coefficients $y_{\mathbf{i}}^{(j)} \in \mathbb{R}$, which from now on are referred to as degrees of freedom (DoFs), i.e.

$$(2.12) \quad y_h|_{\Omega^{(j)}}(\tilde{x}) = \sum_{\mathbf{i} \in \mathbf{I}_0^{(j)}} y_{\mathbf{i}}^{(j)} \hat{\beta}_{\mathbf{i}}^{(j)}(\tilde{x}), \quad \forall j = 1, \dots, N_P.$$

The set $\mathbf{I}_0^{(j)}$ can therefore be seen as the set of DoFs for each patch $\Omega^{(j)}$, $j = 1, \dots, N_P$.

The multi-patch approach is used when the geometric domain Ω cannot be parameterized by a single geometry mapping (2.5) but it also enables us to assume different material models and element types on different patches (cf. [13]) or to undertake a patch-wise local refinement by using different rich bases for the solution spaces of different patches. We note that the patches coincide with the non-overlapping subdomains of a FETI-like method [15]. The challenge in computing an approximation for a PDE problem on a multi-patch geometry Ω lies in the fact that discrete functions $y_h : \Omega \rightarrow \mathbb{R}$ defined by (2.12) are, in general, discontinuous across the patch interfaces. In the following we denote the interface of two patches $\Omega^{(j)}$ and $\Omega^{(k)}$ by

$$\Gamma^{(j,k)} = \partial\Omega^{(j)} \cap \partial\Omega^{(k)}.$$

The set of the index-tupels of all interfaces that are not empty is denoted by

$$\mathcal{C} = \left\{ (j, k) \in \{1, \dots, N_P\}^2 : \Gamma^{(j,k)} \neq \emptyset, j < k \right\}.$$

The condition $j < k$ ensures that each interface is only counted once in \mathcal{C} .

In this paper we assume that the computational domain Ω is represented as a collection of several patches connected along their interfaces with C^0 -continuity. Since the parameter space is the unit cube $\hat{\Omega} = [0, 1]^3$ for each patch, we further assume that each interface $\Gamma^{(j,k)}$ of two patches $\Omega^{(j)}$ and $\Omega^{(k)}$ is always a 2-dimensional surface, which is the image of one entire side of the six sides of the unit cube $\hat{\Omega}$ under both parameterizations $G^{(j)}$ and $G^{(k)}$. For the sake of simplicity, we assume that the two patches which are connected via an interface $\Gamma^{(j,k)}$ have the same orientation in the Cartesian coordinate system, i.e. if we number the sides of the unit cube $\hat{\Omega}$ like a dice for each patch (e.g. the side $\{0\} \times [0, 1] \times [0, 1]$ is referred to as side 1 and $\{1\} \times [0, 1] \times [0, 1]$ as side 6) and for patch $\Omega^{(j)}$ the interface $\Gamma^{(j,k)}$ is the image under $G^{(j)}$ of side 1, then for patch $\Omega^{(k)}$ the interface $\Gamma^{(j,k)}$ is the image under $G^{(k)}$ of side 6. This means that two opposite sides of the dice are always the sides of the patches that form their interface. We also assume that there can only be one interface between two patches.

We say that for $(j, k) \in \mathcal{C}$ the two patches $\Omega^{(j)}$ and $\Omega^{(k)}$ are connected in dimension $d_1 \in \{1, 2, 3\}$ by the interface $\Gamma^{(j,k)}$, if both parameterizations $G^{(j)}$ and $G^{(k)}$ are not fixed in the parameters of the dimensions $d_2, d_3 \in \{1, 2, 3\} \setminus \{d_1\}$, $d_2 \neq d_3$, when mapping to the interface $\Gamma^{(j,k)}$, which means that the dimensions d_2 and d_3 span the interface $\Gamma^{(j,k)}$. In the following, triplets of the variables that depend on these dimensions are written in the order specified by the additional index, so that it can

be understood as a correctly permuted variant of the triplet, i.e. let $d_1 = 3$, $d_2 = 1$, $d_3 = 2$, then $(\tilde{n}_{d_1}^{(j)}, \tilde{n}_{d_2}^{(j)}, \tilde{n}_{d_3}^{(j)})$ is equivalent to $(\tilde{n}_1^{(j)}, \tilde{n}_2^{(j)}, \tilde{n}_3^{(j)})$.

In the following for $(j, k) \in \mathcal{C}$ we will use

$$\mathbf{I}_\Gamma(j, k) = \left\{ \mathbf{i} \in \mathbf{I}_0^{(j)} : \text{supp} \left(\hat{\beta}_{\mathbf{i}}^{(j)} \right) \cap \Gamma^{(j,k)} \neq \emptyset \right\}$$

to denote the set of indices of basis functions on $\Omega^{(j)}$, whose support intersects with the interface $\Gamma^{(j,k)}$ and for $\mathbf{i} \in \mathbf{I}_\Gamma(j, k)$ we say that $y_{\mathbf{i}}^{(j)}$ is associated with the interface $\Gamma^{(j,k)}$. The definition of $\mathbf{I}_\Gamma(k, j)$ is analogous for $(j, k) \in \mathcal{C}$, i.e. for $\mathbf{m} \in \mathbf{I}_\Gamma(k, j)$, $y_{\mathbf{m}}^{(k)}$ is associated with $\Gamma^{(j,k)}$. Because of our assumption about the orientation of the patches and the tensor product structure of the splines, these DoFs can be easily identified. For example, let for $(j, k) \in \mathcal{C}$ the patches $\Omega^{(j)}$ and $\Omega^{(k)}$ be connected in dimension $d = 2$, such that the interface $\Gamma^{(j,k)}$ is located on side 2 of patch $\Omega^{(j)}$ and correspondingly on side 5 of patch $\Omega^{(k)}$, then

$$\begin{aligned} \mathbf{I}_\Gamma(j, k) &= \left\{ \left(i_1^{(j)}, 1, i_3^{(j)} \right) : i_d^{(j)} = 1, \dots, \tilde{n}_d^{(j)}, d \in \{1, 3\} \right\} \subset \mathbb{N}^{\tilde{n}_1^{(j)} \times 1 \times \tilde{n}_3^{(j)}}, \\ \mathbf{I}_\Gamma(k, j) &= \left\{ \left(i_1^{(k)}, \tilde{n}_2^{(k)}, i_3^{(k)} \right) : i_d^{(k)} = 1, \dots, \tilde{n}_d^{(k)}, d \in \{1, 3\} \right\} \subset \mathbb{N}^{\tilde{n}_1^{(k)} \times 1 \times \tilde{n}_3^{(k)}}. \end{aligned}$$

We see, if the two patches $\Omega^{(j)}$ and $\Omega^{(k)}$ are connected in dimension $d_1 \in \{1, 2, 3\}$ by the interface $\Gamma^{(j,k)}$, then $\mathbf{I}_\Gamma(j, k)$ can be understood as the set of the $\tilde{n}_{d_2}^{(j)} \tilde{n}_{d_3}^{(j)}$ many DoFs $y_{\mathbf{I}_\Gamma(j,k)}^{(j)} \in \mathbb{R}^{1 \times \tilde{n}_{d_2}^{(j)} \times \tilde{n}_{d_3}^{(j)}}$ of patch $\Omega^{(j)}$ that lie on the interface $\Gamma^{(j,k)}$.

3. Jump tensors. The strategy of the IETI method [15] for finding an approximation for (1.1) is to determine the coefficients \mathbf{y} of the discrete approximation $y_h \in \Pi V_h$ by solving the following saddle point formulation

$$(3.1) \quad \begin{bmatrix} \mathbf{K} & \mathbf{A}^\top \\ \mathbf{A} & 0 \end{bmatrix} \begin{bmatrix} \mathbf{y} \\ \boldsymbol{\lambda} \end{bmatrix} = \begin{bmatrix} \mathbf{f} \\ 0 \end{bmatrix},$$

where \mathbf{K} is a block diagonal matrix having the local stiffness matrices of each patch on its diagonal, \mathbf{A} is a so-called jump matrix through which the C^0 -continuity is enforced by linear constraints, \mathbf{f} is the source vector and $\boldsymbol{\lambda}$ the corresponding Lagrange multipliers. To transfer this idea to the tensor setup, we think of the system (3.1) as a block system of tensors, where each block has again a block structure. This means

$$(3.2) \quad \mathbf{K} = \begin{bmatrix} K^{(1)} & & \\ & \ddots & \\ & & K^{(N_P)} \end{bmatrix}$$

is a block diagonal tensor and its diagonal blocks $K^{(j)}$, $j = 1, \dots, N_P$, are 3-dimensional stiffness tensors defined by (2.11), corresponding to the bilinear form on each patch $\Omega^{(j)}$. The tensor $\mathbf{y} = [y^{(1)}, \dots, y^{(N_P)}]^\top$ is the unique representation of $y_h : \Omega \rightarrow \mathbb{R}$, whose blocks $y^{(j)} \in \mathbb{R}^{\tilde{n}_1^{(j)} \times \tilde{n}_2^{(j)} \times \tilde{n}_3^{(j)}}$ are the local tensors with the real-valued coefficients of each patch $\Omega^{(j)}$ for (2.12). The source tensor \mathbf{f} has the same structure as \mathbf{y} .

The continuity of the approximation y_h is ensured in (3.1) by a so-called *jump tensor* \mathbf{A} and the Lagrange multipliers $\boldsymbol{\lambda} = [\lambda^{(1)}, \dots, \lambda^{(l)}]^\top$. The jump tensor \mathbf{A} is

also in block structure and has horizontally N_P many block columns and vertically $|\mathcal{C}|$ many block rows, one for each interface. In each block row of \mathbf{A} , all blocks are zero tensors except for two blocks. Let $(j, k) \in \mathcal{C}$, then by applying \mathbf{A} to \mathbf{y} , the C^0 -continuity of $y_h: \Omega \rightarrow \mathbb{R}$ on the interface $\Gamma^{(j,k)}$ is enforced on the DoFs $y^{(j)}$ and $y^{(k)}$ through the corresponding block row of \mathbf{A} with the two non-zero tensors $A_{(j,k)}^{(j)}$ and $A_{(j,k)}^{(k)}$ via

$$(3.3) \quad A_{(j,k)}^{(j)} \cdot y^{(j)} - A_{(j,k)}^{(k)} \cdot y^{(k)} = 0,$$

where \cdot denotes the contracted product over the dimensions $\tilde{n}_1^{(j)} \times \tilde{n}_2^{(j)} \times \tilde{n}_3^{(j)}$. The idea is that the DoFs of one patch should be expressed as a linear combination of the DoFs of the other patch on the interface $\Gamma^{(j,k)}$. We note that other boundary conditions are not incorporated in \mathbf{A} as in [15], since we only consider homogeneous Dirichlet conditions and by using the index sets $\mathbf{I}_0^{(j)}$ the corresponding entries in the local stiffness tensors $K^{(j)}$, $j = 1, \dots, N_P$, are simply eliminated. We further note that $\boldsymbol{\lambda}$ is only unique up to an additive constant of $\ker(\mathbf{A}^\top)$.

As in [15], the tensors $A_{(j,k)}^{(j)}$ and $A_{(j,k)}^{(k)}$ enforce C^0 -continuity by linear constraints on the DoFs $y^{(j)}$ and $y^{(k)}$, which each are located on the interface $\Gamma^{(j,k)}$. For this, the tensor $A_{(j,k)}^{(j)}$ has to address the corresponding DoFs of patch $\Omega^{(j)}$ with indices in $\mathbf{I}_\Gamma(j, k)$. For that we make use of the tensor product structure of the solution space $V_h^{(j)}$. Each DoF $y_{\mathbf{i}}^{(j)}$, which represents the basis function $\hat{\beta}_{\mathbf{i}}^{(j)} \in V_h^{(j)}$, $\mathbf{i} = (i_1, i_2, i_3) \in \mathbf{I}_0^{(j)}$, can be addressed by

$$(3.4) \quad \begin{aligned} y_{\mathbf{i}}^{(j)} &= v_{\mathbf{i}} \cdot y^{(j)}, \\ v_{\mathbf{i}} &= v_{i_1} \otimes v_{i_2} \otimes v_{i_3} \in \mathbb{R}^{(1,1,1) \times (\tilde{n}_1^{(j)}, \tilde{n}_2^{(j)}, \tilde{n}_3^{(j)})}, \\ v_{i_d} &= [0, \dots, 0, 1, 0, \dots, 0] \in \mathbb{R}^{1 \times \tilde{n}_d^{(j)}}, d = 1, 2, 3. \end{aligned}$$

\uparrow
 i_d -th entry

This justifies that for $(j, k) \in \mathcal{C}$ the tensors $A_{(j,k)}^{(m)}$, $m \in \{j, k\}$, have a rank-one representation, i.e.

$$(3.5) \quad A_{(j,k)}^{(m)} = A_{(j,k)}^{(m)(1)} \otimes A_{(j,k)}^{(m)(2)} \otimes A_{(j,k)}^{(m)(3)} \in \mathbb{R}^{(J_1^{(j,k)}, J_2^{(j,k)}, J_3^{(j,k)}) \times (\tilde{n}_1^{(m)}, \tilde{n}_2^{(m)}, \tilde{n}_3^{(m)})}$$

where $A_{(j,k)}^{(m)(d)} \in \mathbb{R}^{J_d^{(j,k)} \times \tilde{n}_d^{(m)}}$, $J_d^{(j,k)}$ is the number of continuity constraints in dimension d , and the entries of these factor matrices depend on the underlying interface $\Gamma^{(j,k)}$. To simplify the notation, we will omit the index (j, k) in the following. When transposing \mathbf{A} , the block structure of \mathbf{A} is transposed as in the matrix case and in addition all factor matrices $A^{(m)(d)}$, $d \in \{1, 2, 3\}$, in (3.5) are transposed.

The C^0 -continuity of the discrete approximation $y_h: \Omega \rightarrow \mathbb{R}$ can now be enforced by choosing suitable factor matrices in (3.5). Their entries depend on which side of the unit cube the interface $\Gamma^{(j,k)}$ of the respective patch is located and the relationship between $y_{\mathbf{I}_\Gamma(j,k)}^{(j)}$ and $y_{\mathbf{I}_\Gamma(k,j)}^{(k)}$. By exploiting the tensor product structure of $V_h^{(m)}$, $m \in \{j, k\}$, we can split the C^0 -continuity condition on the interface $\Gamma^{(j,k)}$ into

1-dimensional C^0 -continuity conditions and thus formulate the corresponding linear constraints in the factor matrix $A^{(m)(d)}$ for each dimension $d \in \{1, 2, 3\}$.

For $(j, k) \in \mathcal{C}$ let $\Omega^{(j)}$ and $\Omega^{(k)}$ be connected by the interface $\Gamma^{(j,k)}$ in dimension $d_1 \in \{1, 2, 3\}$. Then $\mathbf{I}_\Gamma(j, k)$ and $\mathbf{I}_\Gamma(k, j)$ are 1-dimensional in dimension d_1 , which means that for each patch all basis functions on this interface $\hat{\beta}_{\mathbf{I}_\Gamma(j,k)}^{(j)}$, and thus the discrete function y_h , are constructed by only one univariate spline in dimension d_1 , see (2.6). As this univariate spline must be located on one side of the unit cube for each patch in dimension d_1 and based on our assumption about the orientation of the patches, this is the first univariate spline for one patch and the last univariate spline for the other patch in dimension d_1 . All basis functions on the interface $\Gamma^{(j,k)}$ of the corresponding patch have this one univariate spline in (2.6), and to ensure C^0 -continuity on that interface, the DoFs of both patches that depend on this univariate spline must match in dimension d_1 . From (3.4), we can identify all DoFs of the basis functions in dimension d_1 for both patches $\Omega^{(j)}$ and $\Omega^{(k)}$ by using a row vector, i.e. $A^{(m)(d_1)} \in \mathbb{R}^{1 \times \tilde{n}_{d_1}^{(m)}}$, $m \in \{j, k\}$. This row vector contains only zeros except for one 1, which is either the first or the last entry of the vector for the corresponding patch, which depends on which of the two sides of the unit cube of the respective patch in dimension d_1 the interface $\Gamma^{(j,k)}$ is located. When we think of a dice again and for patch $\Omega^{(j)}$ the interface is located on side 1 and for patch $\Omega^{(k)}$ on side 6, then $d_1 = 1$ and we have

$$\begin{aligned} A^{(j)(1)} &= [1, 0, \dots, 0] \in \mathbb{R}^{1 \times \tilde{n}_1^{(j)}}, \\ A^{(k)(1)} &= [0, \dots, 0, 1] \in \mathbb{R}^{1 \times \tilde{n}_1^{(k)}}, \end{aligned}$$

as d_1 -th factor matrix for $A^{(j)}$ and $A^{(k)}$ in (3.5). This addresses the DoFs on the interface on the corresponding side of the respective patch in the dimension d_1 of the dice due to the tensor product structure. We note that we multiply one of the two factor matrices $A^{(j)(d_1)}$ or $A^{(k)(d_1)}$ by -1 , since we want to subtract the resulting tensors from each other as in (3.3).

The factor matrices in (3.5) for dimension $d_l \in \{1, 2, 3\} \setminus \{d_1\}$, $l \in \{2, 3\}$, depend on whether the patches $\Omega^{(j)}$ and $\Omega^{(k)}$ are *fully matching* (cf. [15]) in this dimension d_l on the interface $\Gamma^{(j,k)}$ or not.

If the patches $\Omega^{(j)}$ and $\Omega^{(k)}$ are fully matching on $\Gamma^{(j,k)}$ in dimension $d_l \in \{1, 2, 3\} \setminus \{d_1\}$, $l \in \{2, 3\}$, then the knot vector $\xi_{d_l}^{(j)}$ is affinely related to the knot vector $\xi_{d_l}^{(k)}$ and the corresponding weights and degrees are equal. In the following, we will use the familiar term *conforming*. With our assumption about the orientation of the patches, the two knot vectors actually match in this case, which in turn implies, that $\mathbb{S}_{\xi_{d_l}^{(j)}}^{(j)} = \mathbb{S}_{\xi_{d_l}^{(k)}}^{(k)}$ and $\tilde{n}_{d_l}^{(j)} = \tilde{n}_{d_l}^{(k)}$ holds. This means that the univariate factors of the basis functions of both patches $\Omega^{(j)}$ and $\Omega^{(k)}$ coincide in (2.6) for this dimension d_l on the interface $\Gamma^{(j,k)}$. To ensure C^0 -continuity of the approximation, the d_l -th factor matrix in (3.5) for both patches must be a square Boolean matrix $A^{(m)(d_l)} \in \mathbb{R}^{\tilde{n}_{d_l}^{(m)} \times \tilde{n}_{d_l}^{(m)}}$, $m \in \{j, k\}$, whose rows are the vectors $v_{i_{d_l}} \in \mathbb{R}^{1 \times \tilde{n}_{d_l}^{(m)}}$ for dimension d_l in (3.4), which address the corresponding DoFs on the interface $\Gamma^{(j,k)}$. With our assumption about the orientation, these factor matrices in (3.5) are for both patches $\Omega^{(j)}$ and $\Omega^{(k)}$ the identity matrix, i.e. $A^{(j)(d_l)} = A^{(k)(d_l)} = \mathbb{I} \in \mathbb{R}^{\tilde{n}_{d_l}^{(j)} \times \tilde{n}_{d_l}^{(j)}}$.

If the patches $\Omega^{(j)}$ and $\Omega^{(k)}$ are not fully matching or *nonconforming* in dimension

$d_l \in \{1, 2, 3\} \setminus \{d_1\}$, $l \in \{2, 3\}$, but the knot vector $\xi_{d_l}^{(j)}$ is obtained from the knot vector $\xi_{d_l}^{(k)}$ by one step of uniform h-refinement, then the univariate spline spaces $\mathbb{S}_{\xi_{d_l}^{(j)}}^{(j)}$ and $\mathbb{S}_{\xi_{d_l}^{(k)}}^{(k)}$ no longer coincide with each other and $\tilde{n}_{d_l}^{(j)} \neq \tilde{n}_{d_l}^{(k)}$. In [15] it was shown for the 2-dimensional case, where the interface is a 1-dimensional edge, that the DoFs of the finer patch $\Omega^{(j)}$ can be expressed as a linear combination of the DoFs of the coarser patch $\Omega^{(k)}$ on the interface $\Gamma^{(j,k)}$. We adopt this approach, which means that $\forall (i_{d_1}^{(j)}, i_{d_l}^{(j)}, i_{d_p}^{(j)}) \in \mathbf{I}_\Gamma(j, k)$

$$(3.6) \quad y_{(i_{d_1}^{(j)}, i_{d_l}^{(j)}, i_{d_p}^{(j)})}^{(j)} = \sum_{i_{d_l}^{(k)}=1}^{\tilde{n}_{d_l}^{(k)}} Z_{i_{d_l}^{(j)}, i_{d_l}^{(k)}} y_{(i_{d_1}^{(k)}, i_{d_l}^{(k)}, i_{d_p}^{(k)})}^{(k)}, \quad (i_{d_1}^{(k)}, i_{d_l}^{(k)}, i_{d_p}^{(k)}) \in \mathbf{I}_\Gamma(k, j),$$

must hold to ensure C^0 -continuity, where the linear coefficients $Z \in \mathbb{R}^{\tilde{n}_{d_l}^{(j)} \times \tilde{n}_{d_l}^{(k)}}$ can be obtained from the formula for h-refinement of B-spline basis functions (cf. [30, Section 5.3]). We note that the index $i_{d_l}^{(m)} \in \{1, \tilde{n}_{d_l}^{(m)}\}$, $m \in \{j, k\}$, on both sides in (3.6) is fixed and given by the location of the interface $\Gamma^{(j,k)}$ and for simplicity we assume that the patches $\Omega^{(j)}$ and $\Omega^{(k)}$ are conforming in dimension d_p , which is why we can assume that the index in dimension d_p is the same. If the patches are nonconforming in dimension d_p and the patch $\Omega^{(j)}$ is finer in this dimension, then this would result in a double sum in (3.6), so that the DoFs of the finer patch $\Omega^{(j)}$ can also be represented as a linear combination of the DoFs of the coarser patch $\Omega^{(k)}$. This means that the number of continuity constraints in dimension d_l is given by the number of univariate splines of the finer patch $\Omega^{(j)}$, i.e. $A^{(j)(d_l)} \in \mathbb{R}^{\tilde{n}_{d_l}^{(j)} \times \tilde{n}_{d_l}^{(j)}}$ and $A^{(k)(d_l)} \in \mathbb{R}^{\tilde{n}_{d_l}^{(j)} \times \tilde{n}_{d_l}^{(k)}}$. The factor matrix $A^{(j)(d_l)}$ of the finer patch $\Omega^{(j)}$ is again a Boolean matrix, which addresses with its rows the corresponding DoFs on the interface $\Gamma^{(j,k)}$ as in (3.4). With our assumption about the orientation of the patches, we can choose for that the identity matrix $\mathbb{I} \in \mathbb{R}^{\tilde{n}_{d_l}^{(j)} \times \tilde{n}_{d_l}^{(j)}}$. The factor matrix $A^{(k)(d_l)}$ of the coarser patch $\Omega^{(k)}$ is given by the coefficients matrix, i.e. $A^{(k)(d_l)} = Z$.

4. IETI-based low-rank method. We now discuss how to compute an approximate solution of (3.1) to obtain the linear coefficients $y^{(j)} \in \mathbb{R}^{\tilde{n}_1^{(j)} \times \tilde{n}_2^{(j)} \times \tilde{n}_3^{(j)}}$ for the patch-wise representation (2.12) of the discrete approximation $y_h: \Omega \rightarrow \mathbb{R}$ of (1.1). We consider this here using MATLAB. An extended block AMEN method (implemented as `amen_block_solve.m` in the TT-TOOLBOX [24]), which allows us to solve large systems while preserving the block structure without assembling the whole equation system and returns the solution in a low-rank TT format (cf. [2], [9]), could be used for solving (3.1), but our experiments have shown that this inevitably leads to the complication, that all blocks in \mathbf{K} and \mathbf{A} must have the same size for this solver. An alternative would be to fill the blocks that are too small with zeros in the corresponding entries, but this would greatly impair numerical stability and the performance of the method is not competitive.

As in [15], our approach follows the idea of a FETI-like method by eliminating the primal variables \mathbf{y} from the system (3.1) and solving for the dual variables $\boldsymbol{\lambda}$. The primal variables \mathbf{y} can then be easily recovered from the dual variables $\boldsymbol{\lambda}$. We achieve this by solving the Schur complement of (3.1), i.e. we search for $\boldsymbol{\lambda} = [\lambda^{(1)}, \dots, \lambda^{(l)}]^\top$

that solves

$$(4.1) \quad \mathbf{A} \mathbf{K}^{-1} \mathbf{A}^\top \boldsymbol{\lambda} = \mathbf{A} \mathbf{K}^{-1} \mathbf{f}.$$

All blocks \mathbf{A} , \mathbf{K} , \mathbf{f} and $\boldsymbol{\lambda}$ have the same structure as before and are in TT format. We note that tensors and tensor matrices in canonical format (such as (2.8) and (3.5)) can easily be converted to TT format (cf. [22]). Obviously, the number of variables in (4.1) is smaller, since we only solve for the Lagrange multipliers $\boldsymbol{\lambda}$ and each block of $\boldsymbol{\lambda}$ represents an interface $\Gamma^{(j,k)}$ with $J_{d_2}^{(j,k)} J_{d_3}^{(j,k)}$ many linear constraints, where $J_{d_l}^{(j,k)} = \max\left(\left\{\tilde{n}_{d_l}^{(j)}, \tilde{n}_{d_l}^{(k)}\right\}\right)$, $l \in \{2, 3\}$, since $J_{d_1}^{(j,k)} = 1$.

We find an approximate solution $\boldsymbol{\lambda}^*$ of (4.1) using a tensor block version of TT-GMRES (implemented as `tt_gmres_block.m` in [24], cf. [8]). This method is in contrast to the block AMEN method tensor-matrix free, i.e. we can define the linear operator $\mathbf{A} \mathbf{K}^{-1} \mathbf{A}^\top$ as a function handle and filling with zeros is not necessary. When solving (4.1), we take advantage of the fact that the blocks of $\boldsymbol{\lambda}$ can be represented as 2-dimensional tensors in order to simplify the problem, since these tensors are only 1-dimensional in the dimension d_1 in which the two corresponding patches are connected, i.e. $\lambda^{((j,k))} \in \mathbb{R}^{J_{d_1}^{(j,k)} \times J_{d_2}^{(j,k)} \times J_{d_3}^{(j,k)}} = \mathbb{R}^{1 \times J_{d_2}^{(j,k)} \times J_{d_3}^{(j,k)}} \cong \mathbb{R}^{J_{d_2}^{(j,k)} \times J_{d_3}^{(j,k)}}$. Therefore, the TT-GMRES is applied to a 2-dimensional linear block system in our setup, which reduces the complexity. When applying the function handle of the linear operator $\mathbf{A} \mathbf{K}^{-1} \mathbf{A}^\top$ on $\boldsymbol{\lambda}$, each block of $\boldsymbol{\lambda}$ is first reshaped into 3-dimensional tensors using the `reshape.m` function of the `TT-TOOLBOX`, then the actual linear system is applied and finally all blocks of $\boldsymbol{\lambda}$ are reshaped back into 2-dimensional tensors. When applying \mathbf{K}^{-1} within the function handle, the patch-wise given linear systems are solved using the standard AMEN method (implemented as `amen_solve2.m` in [24]).

Although the system (4.1) is smaller than the original system (3.1), preconditioners are still necessary to compute the variables $\boldsymbol{\lambda}$ in a reasonable number of iterations. This is because the system (4.1) is generally ill-conditioned. We use a block diagonal tensor matrix with $|\mathcal{C}|$ many 3-dimensional tensor matrices as diagonal blocks as a left preconditioner, i.e.

$$(4.2) \quad \mathbf{P}^{-1} \mathbf{A} \mathbf{K}^{-1} \mathbf{A}^\top \boldsymbol{\lambda} = \mathbf{P}^{-1} \mathbf{A} \mathbf{K}^{-1} \mathbf{f},$$

which we apply to the iterate $\boldsymbol{\lambda}^{(k)}$ after applying the linear operator $\mathbf{A} \mathbf{K}^{-1} \mathbf{A}^\top$ but before reshaping back to 2-dimensional tensors in the function handle.

For $(j, k) \in \mathcal{C}$ let $\Omega^{(j)}$ and $\Omega^{(k)}$ be connected by the interface $\Gamma^{(j,k)}$ in dimension $d_1 \in \{1, 2, 3\}$ and assuming that the patch $\Omega^{(j)}$ is at least in one dimension $d_l \in \{1, 2, 3\} \setminus \{d_1\}$, $l \in \{2, 3\}$, finer than the patch $\Omega^{(k)}$. Then we explicitly set the diagonal blocks of \mathbf{P}^{-1} with respect to the Lagrange multipliers of the interface $\Gamma^{(j,k)}$ as

$$(4.3) \quad P^{((j,k))} = A_{(j,k)}^{(j)} \cdot K^{(j)} \cdot A_{(j,k)}^{(j)\top} \in \mathbb{R}^{(1, J_{d_2}^{(j,k)}, J_{d_3}^{(j,k)}) \times (1, J_{d_2}^{(j,k)}, J_{d_3}^{(j,k)})},$$

where $K^{(j)}$ is the low-rank stiffness tensor of patch $\Omega^{(j)}$ and $A_{(j,k)}^{(j)}$ is given by (3.5), both in TT format. Here \cdot denotes again a contracted product, namely the product of two TT matrices (cf. [22]). We note that it is important that we use in (4.3) the information from the finer patch $\Omega^{(j)}$. In the conforming case, it has been shown that we can use the information from either patch and get similar results for the resulting two preconditioners.

5. A PDE-constrained optimization model problem. We now want to discuss the discretization in both time and space of the optimization problem given on (1.2) to (1.5), resulting in a large saddle point problem [3, 11]. Using an implicit Euler scheme for the time discretization of the PDE and the rectangle rule for the objective function leads to the time-discrete problem, which we then discretize in space using a Galerkin-based spatial discretization, which in turn leads to the discrete quadratic problem

$$\begin{aligned} \min_{y,u} \quad & \sum_{\ell=1}^{N_t} \frac{\tau}{2} \left((y_\ell - \hat{y}_\ell)^\top M (y_\ell - \hat{y}_\ell) + \alpha u_\ell^\top M u_\ell \right) \\ \text{s.t.} \quad & \frac{M y_\ell - M y_{\ell-1}}{\tau} + K y_\ell = M u_\ell \quad \text{for } \ell = 1, \dots, N_t, \end{aligned}$$

with the number of time steps N_t corresponding to the time step size $\tau = T/N_t$. For the general case, M and K can be understood as mass or stiffness matrix of the corresponding geometry and all boundary conditions (1.4) are incorporated in M and K . The states are collected in a block vector $y = [y_1, \dots, y_{N_t}]^\top$ and similarly for the control u and the desired state \hat{y} .

Such problems typically lead to saddle point systems as discussed in [3, 11]. We get to such a formulation by applying a Lagrangian formalism using a multiplier block vector $\mu = [\mu_1, \dots, \mu_{N_t}]^\top$ such that the *Lagrangian* of the problem reads as

$$(5.1) \quad \mathcal{L}(y, u, \mu) = \sum_{\ell=1}^{N_t} \left(\frac{\tau}{2} \left((y_\ell - \hat{y}_\ell)^\top M (y_\ell - \hat{y}_\ell) + \alpha u_\ell^\top M u_\ell \right) + \mu_\ell^\top (M y_\ell - M y_{\ell-1} + \tau K y_\ell - \tau M u_\ell) \right).$$

Taking the derivative with respect to state y , control u and Lagrange multiplier μ leads to the system

$$(5.2) \quad \begin{bmatrix} \tau \mathcal{M} & 0 & \mathcal{K}^\top \\ 0 & \tau \alpha \mathcal{M} & -\tau \mathcal{M} \\ \mathcal{K} & -\tau \mathcal{M} & 0 \end{bmatrix} \begin{bmatrix} y \\ u \\ \mu \end{bmatrix} = \begin{bmatrix} \tau \mathcal{M} \hat{y} \\ 0 \\ 0 \end{bmatrix},$$

where $\mathcal{M} = \mathbb{I} \otimes M$ and $\mathcal{K} = \mathbb{I} \otimes \tau K + C \otimes M$, using the identity matrix $\mathbb{I} \in \mathbb{R}^{N_t \times N_t}$ and C is representing the Euler scheme via

$$C = \begin{bmatrix} 1 & 0 & 0 & \dots & 0 \\ -1 & 1 & 0 & \dots & 0 \\ 0 & -1 & 1 & \dots & 0 \\ \vdots & & \ddots & \ddots & \\ 0 & \dots & 0 & -1 & 1 \end{bmatrix}.$$

Note that in this derivation we used the same spline spaces for the state and control. It is also possible to have a different discretization for the control and this would make the system solver we use in the low-rank method more involved (cf. [5]). The resulting equation system (5.2) is a saddle point problem as described in [3, 33, 28].

We now define the linear system (5.2) for multi-patch geometries, enforcing C^0 -continuity for the state y and the Lagrange multiplier μ , but not for the control u ,

since this is an algebraic variable (cf. [12]). We now include jump tensors as in the case of the elliptic problem. By introducing Lagrange multipliers with respect to the continuity constraints for y and μ we obtain

$$(5.3) \quad \begin{bmatrix} \tau\bar{M} & 0 & 0 & \bar{K}^\top & \bar{A} \\ 0 & 0 & 0 & \bar{A}^\top & 0 \\ 0 & 0 & \tau\alpha\bar{M} & -\tau\bar{M} & 0 \\ \bar{K} & \bar{A}^\top & -\tau\bar{M} & 0 & 0 \\ \bar{A} & 0 & 0 & 0 & 0 \end{bmatrix} \begin{bmatrix} y \\ \lambda_y \\ u \\ \mu \\ \lambda_\mu \end{bmatrix} = \begin{bmatrix} \tau\mathcal{M}\hat{y} \\ 0 \\ 0 \\ 0 \\ 0 \end{bmatrix},$$

where \bar{M} and \bar{K} are block diagonal tensors as in (3.2) with diagonal blocks

$$\bar{M}^{(j)} = \mathbb{I} \otimes M^{(j)}, \quad \bar{K}^{(j)} = \mathbb{I} \otimes \tau K^{(j)} + C \otimes M^{(j)}, \quad j = 1, \dots, N_p,$$

where $M^{(j)}$ is defined by (2.10) and $K^{(j)}$ by (2.11). Since the continuity should apply for all time steps, we set each block of this jump tensor \bar{A} to $\mathbb{I} \otimes A_{(j,k)}^{(m)}$ where $A_{(j,k)}^{(m)}$, $(j, k) \in \mathcal{C}$, $m \in \{j, k\}$, is defined as in section 3. The resulting saddle point problem (5.3) typically becomes very large, depending on the number of time steps and refinement in the spatial discretization which is why we are solving the Schur complement for u

$$(5.4) \quad \left(\tau\alpha\bar{M} + \tau^3 \begin{bmatrix} \bar{M} & 0 \\ \overbrace{\begin{bmatrix} \bar{K} & \bar{A}^\top \\ \bar{A} & 0 \end{bmatrix}^{-\top}}^{=\bar{\mathcal{K}}^{-\top}} & \begin{bmatrix} \bar{M} & 0 \\ 0 & 0 \end{bmatrix} \overbrace{\begin{bmatrix} \bar{K} & \bar{A}^\top \\ \bar{A} & 0 \end{bmatrix}^{-1}}^{=\bar{\mathcal{K}}^{-1}} & \begin{bmatrix} \bar{M} \\ 0 \end{bmatrix} \end{bmatrix} \right) u = \tau^2 \begin{bmatrix} \bar{M} & 0 \\ \bar{A} & 0 \end{bmatrix}^{-\top} \begin{bmatrix} \bar{M} \\ 0 \end{bmatrix} \hat{y},$$

where the control is defined by $u = [u^{(1)}, \dots, u^{(N_p)}]^\top$. The blocks of u are tensors of the form $u^{(j)} \in \mathbb{R}^{\tilde{n}_1^{(j)} \times \tilde{n}_2^{(j)} \times \tilde{n}_3^{(j)} \times N_t}$ for each patch $\Omega^{(j)}$ and for all time steps. The state y and multiplier μ can be easily recovered from the computed u .

We consider solving (5.4) using MATLAB. In order to compute u , we first transform all tensors in TT format and then use again the tensor block version of TT-GMRES. The application of matrix vector product in (5.4) is computed by applying one operator after the other, which means that when applying (5.4) we have to solve a linear system once with $\bar{\mathcal{K}}$ and once with $\bar{\mathcal{K}}^\top$, for which we use the approach described in section 4 with the preconditioner described there. To reduce the number of iterations of TT-GMRES, we apply the left preconditioner \mathcal{P} whose block with respect to the patch $\Omega^{(j)}$ is defined as

$$(5.5) \quad \mathcal{P}^{(j)} = \tau\alpha\mathbb{I} \otimes \bigotimes_{d=1}^3 M_{r_d}^{(j)(d)}.$$

Here $M_{r_d}^{(j)(d)}$ is one of the factor matrices in (2.11) of $M^{(j)}$ and r_d is chosen so that the norm of $M_{r_d}^{(j)(d)}$ is the largest for all $M_r^{(j)(d)}$, $r = 1, \dots, R$, in this dimension d .

Note that since we are using an iterative solver, to apply the operator of (5.4) in every iteration a flexible method such as FGMRES will be ideally suited and we will tailor our approach in future research to this method as well designing a more sophisticated preconditioning strategy for this system.

6. Numerical experiments. We now present the results of our numerical experiments. First, we investigate the error and performance of the method presented in section 4 with respect to different refinement levels and different solution tolerances. Secondly, we investigate the robustness of our in section 5 proposed method with respect to the penalty parameter α . The experiments are conducted on two B-spline and one NURBS geometry with corresponding source functions or desired states for conforming and nonconforming patch discretizations. We point out that we restrict ourselves to low-rank multi-patch geometries, which means that the assembled mass and stiffness tensors of the individual patches have a low rank in the representation given by (2.10) and (2.11) (cf. [5]). This choice of geometry allows us, at least for the B-spline geometries, to further reduce the cost of the assembly process. In more detail, we do not require a rich spline space for the interpolation of the weight functions as then refinement only takes place for the basis of the solution space.

For our numerical experiments we used MATLAB R2022b on a desktop computer with an AMD Ryzen 5 5600X 6-core processor with 16 GB of RAM. Both geometries and specific functions from the GEOPDES 3.0 toolbox [35] with the aid of the NURBS TOOLBOX [32] were used. Computations in the TT-format were carried out using the TT-TOOLBOX [24].

6.1. Elliptic Problem. Let N_{DoFs} denote the total number of DoFs for the multi-patch geometry Ω and $N_{DoFs}^{(j)}$ the number of DoFs of patch $\Omega^{(j)}$ of Ω . Thus, we define the relative \mathcal{L}^2 -error to the analytical solution on a single patch and on the whole geometry as

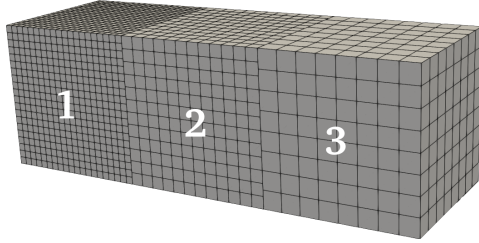
$$(6.1) \quad R^{(j)}(y_h, y_{sol}) = \frac{\|y_h|_{\Omega^{(j)}} - y_{sol}|_{\Omega^{(j)}}\|_{\mathcal{L}^2(\Omega^{(j)})}}{\|y_{sol}|_{\Omega^{(j)}}\|_{\mathcal{L}^2(\Omega^{(j)})}},$$

$$R(y_h, y_{sol}) = \sum_{j=1}^{N_p} \frac{N_{DoFs}^{(j)}}{N_{DoFs}} R^{(j)}(y_h, y_{sol}),$$

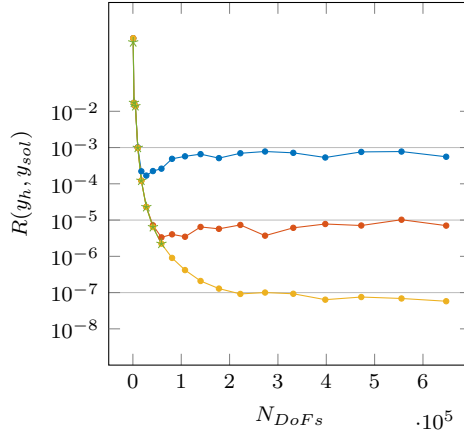
where $y_h|_{\Omega^{(j)}}$ denotes the discrete approximation described by (2.12) for patch $\Omega^{(j)}$, $y_{sol}: \Omega \rightarrow \mathbb{R}$ is the analytical solution and $\|\cdot\|_{\mathcal{L}^2(\Omega^{(j)})}$ denotes the usual \mathcal{L}^2 -norm.

For each numerical experiment we measure the error to the analytical solution given by (6.1), the number of iterations of the solver and the total time needed to compute the approximation, depending on different refinements of the solution space and different tolerances. Refinement in the conforming case is to be understood as starting with the original spline basis given by the geometry and then performing one step of uniform h -refinement with an increasing number of knots to be inserted between two existing knots in each dimension. In the nonconforming case, we do the same, but then undertake another one or two steps of uniform h -refinement for certain patches, in which only a single knot is inserted between two existing knots. Since we have to rely on functions of the toolbox GEOPDES 3.0 [35] for the error calculation and for that we have to use the full coefficient vector, i.e. $\text{vec}(y^{(j)}) \in \mathbb{R}^{\tilde{n}_1^{(j)} \tilde{n}_2^{(j)} \tilde{n}_3^{(j)}}$, this is currently our limiting factor for further increasing the number of DoFs. Here, ε refers to the tolerance for solving the weight function interpolation system (2.9) within `amen_block_solve.m` (cf. [5]). For solving (4.2) we use `tt_gmres_block.m`, where we set `max_iters` to 10, `restart` to 20, and `tol` to $\varepsilon \cdot 10^2$. For solving the local linear systems defined by $K^{(j)}$ inside (4.2) we use `amen_solve2.m`¹. For the

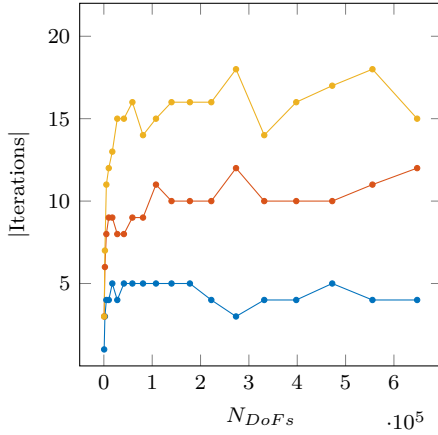
¹with parameters `nswp` = 20, `kickrank` = 2 and `tol` = $\varepsilon \cdot 10$



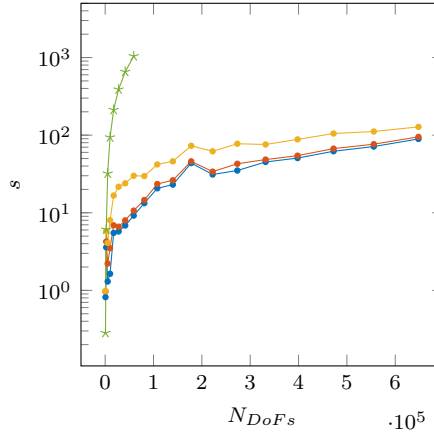
(a) 3 cubes connected next to each other.



(b) Relative \mathcal{L}^2 -error on Ω .



(c) Number of iterations.



(d) Total time in seconds s .



Fig. 1: Performance for different refinements and tolerances on the conforming multi-patch geometry with 3 cubes shown in 1a with (6.2) as analytical solution.

conforming cases, we compare the error and time of our method with the results of an approximation computed using GEOPDES 3.0, which is limited to conforming geometries.

We first study the multi-patch B-spline geometry shown in Figure 1a where the analytical solution of (1.1) for this experiment is given by

$$(6.2) \quad y_{sol}(x, y, z) = \sin(\sin(y\pi) \sin(z2\pi) \sin(x\pi)) \sin(y\pi) \sin(z2\pi) \sin(x\pi).$$

We use B-splines of degree 5 in both the conforming case and the nonconforming case. In the conforming case, we start with $N_{DoFs}^{(j)} = 216$ and we increase the number of knots to be inserted until we reach $N_{DoFs}^{(j)} = 216.000$ DoFs for $j = 1, 2, 3$. In

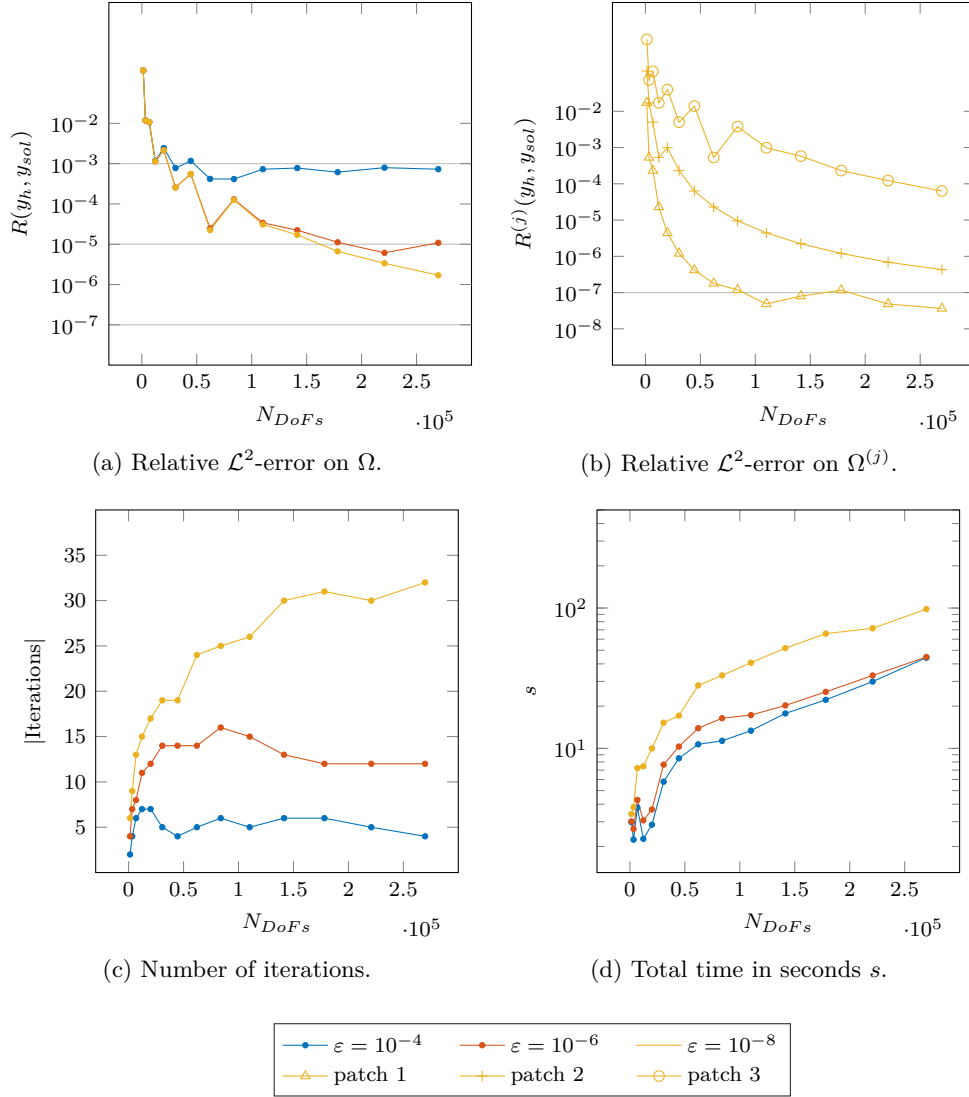


Fig. 2: Performance for different refinements and tolerances on the nonconforming multi-patch geometry with 3 cubes shown in 1a with (6.2) as analytical solution.

the nonconforming case, we start with the division $N_{DoFs}^{(1)} = 729$, $N_{DoFs}^{(2)} = 343$, $N_{DoFs}^{(3)} = 216$ and end with $N_{DoFs}^{(1)} = 226.981$, $N_{DoFs}^{(2)} = 35.937$, $N_{DoFs}^{(3)} = 6.859$.

Figure 1b shows the relative \mathcal{L}^2 -error $R(y_h, y_{sol})$ on the whole multi-patch geometry Ω for different ϵ and depending on N_{DoFs} . We see at a certain point, further refinement no longer reduces the error for a given fixed tolerance ϵ , since for $\epsilon = 10^{-4}$ the error $R(y_h, y_{sol})$ does not decrease further after the sixth step of increasing N_{DoFs} , but increases and approaches $\epsilon = 10^{-3}$. Similar can be recognised for $\epsilon = 10^{-6}, 10^{-8}$. We can derive from that, that if the error should be reduced by refinement, this must be done together with a calibration of the tolerance ϵ . We can also see in Figure 1b the error of the approximation generated using GEOPDES 3.0, where we are only able to

compute the solutions until the eighth step of increasing N_{DoFs} , due to higher memory requirements. Nevertheless, our method and GEOPDES 3.0 show high agreement. We can derive from the number of iterations shown in Figure 1c that they depend mainly on ε and we see in Figure 1d that the timing for our method shows a very benign growth with increasing number of N_{DoFs} . In summary, it can be deduced from the results that the error behaviour of the method presented in section 4 shows very mild dependence on the number of degrees of freedom but that also a higher accuracy requires further adjustment of the tolerance levels.

Figure 2 shows a similar set of results for the nonconforming case. The decrease of the error $R(y_h, y_{sol})$ is slower than in the conforming case, which is due to the fact that the patches are refined differently and therefore error decrease at different rates. This is well illustrated in Figure 2b. Here the error $R^{(j)}(y_h, y_{sol})$ is shown for the tolerance $\varepsilon = 10^{-8}$ on a single patch $\Omega^{(j)}$ depending on N_{DoFs} . In our numerical tests it has been shown that an actual difference in the error $R^{(j)}(y_h, y_{sol})$ for the patches with different refinement is only recognizable for higher tolerances. Here too, the error behaviour is as expected. The patch with the highest refinement, patch 1 in Figure 1a, converges at the fastest rate to an error of 10^{-7} . It is to be expected that the error for the other two patches will correspond to this if further refinements are carried out. The number of iterations shown in Figure 2c is higher than in the conforming case, but this is due to the fact that the system (4.2) is more complex, since the factor matrices in (3.5) are not just Boolean matrices in that case, but have more structure. Nevertheless, the method converges in a satisfying time also in the nonconforming case.

The second B-spline geometry consisting of four cuboids connected to a cube is shown in Figure 3a, where the analytical solution is given by

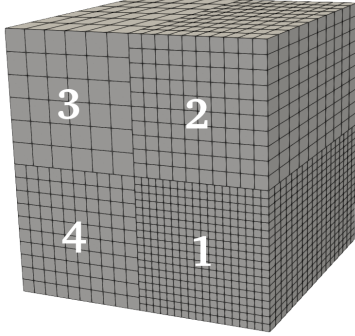
$$(6.3) \quad y_{sol}(x, y, z) = \sin(x 3\pi) \sin(y \pi) \sin(z \pi).$$

We use B-splines of degree 3 in both the conforming case (results in Figure 3) and the nonconforming case (results in Figure 4). In the conforming case, we start with $N_{DoFs}^{(j)} = 64$ and end with $N_{DoFs}^{(j)} = 373.248$ for $j = 1, \dots, 4$. In the nonconforming case, we start with $N_{DoFs}^{(1)} = 343$, $N_{DoFs}^{(2)} = 125$, $N_{DoFs}^{(4)} = 64$ and end with $N_{DoFs}^{(1)} = 357.911$, $N_{DoFs}^{(2)} = 50.653$, $N_{DoFs}^{(3)} = 8000$. We observe similar trends for this domain. It is clear that the iteration numbers do increase for the nonconforming domain and that the tolerance for an increased number of DoFs also needs further adjustment of the tolerances as stagnation of accuracy can be observed when the tolerances are not decreased accordingly.

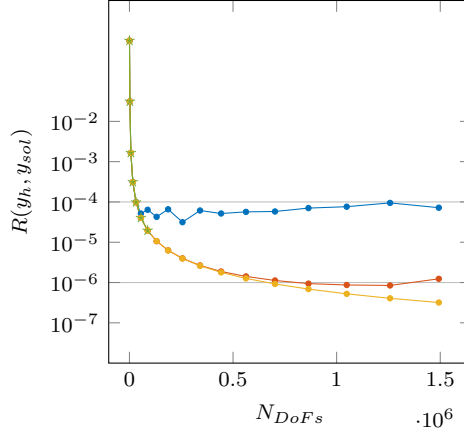
The last two test cases are studied on a NURBS geometry shown in Figure 5a consisting of two vertically stacked annuli. The analytical is given by:

$$(6.4) \quad y_{sol}(x, y, z) = (x^2 + y^2 - 1) (x^2 + y^2 - 4) x y z (z - 2).$$

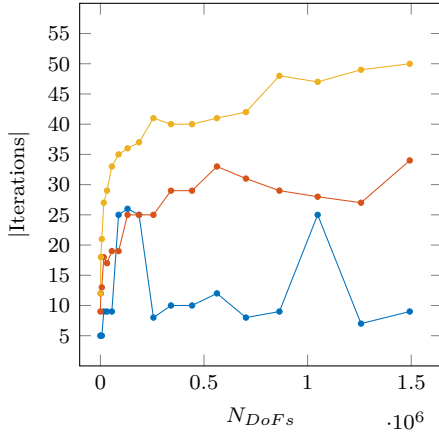
We use B-splines of degree 3 in both the conforming case (results in Figure 5) and the nonconforming case (results in Figure 6). In the conforming case, we start with $N_{DoFs}^{(j)} = 64$ and end with $N_{DoFs}^{(j)} = 438.976$ for $j = 1, 2$. In the nonconforming case, we start with $N_{DoFs}^{(1)} = 125$, $N_{DoFs}^{(2)} = 64$ and end with $N_{DoFs}^{(1)} = 456.533$, $N_{DoFs}^{(2)} = 64.000$. We observe similar results here too.



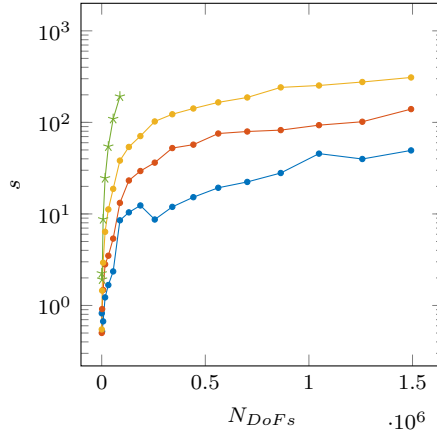
(a) 4 cuboids connected to form a cube.



(b) Relative \mathcal{L}^2 -error on Ω .



(c) Number of iterations.



(d) Total time in seconds s .



Fig. 3: Performance for different refinements and tolerances on the conforming multi-patch geometry with 4 cuboids shown in 3a with (6.3) as analytical solution.

6.2. Optimal control. We now illustrate the performance of our low-rank approach in section 5 for the optimal control problem (1.2) to (1.5) using the following desired state

$$(6.5) \quad \hat{y}(x, y, z; t) = e^{\frac{1}{t+1}} y_{sol}(x, y, z).$$

and we set $T = 1$ and $N_t = 10$. Our main goal is to illustrate the robustness of our method with respect to changes in the penalty parameter α . We solve (5.4) using `tt_gmres_block.m`, where we set `max_iters` to 10, `restart` to 20, and `tol` to 10^{-5} . We solve the inner linear systems $\tilde{\mathcal{K}}$ and $\tilde{\mathcal{K}}^\top$ with the approach described in section 4,

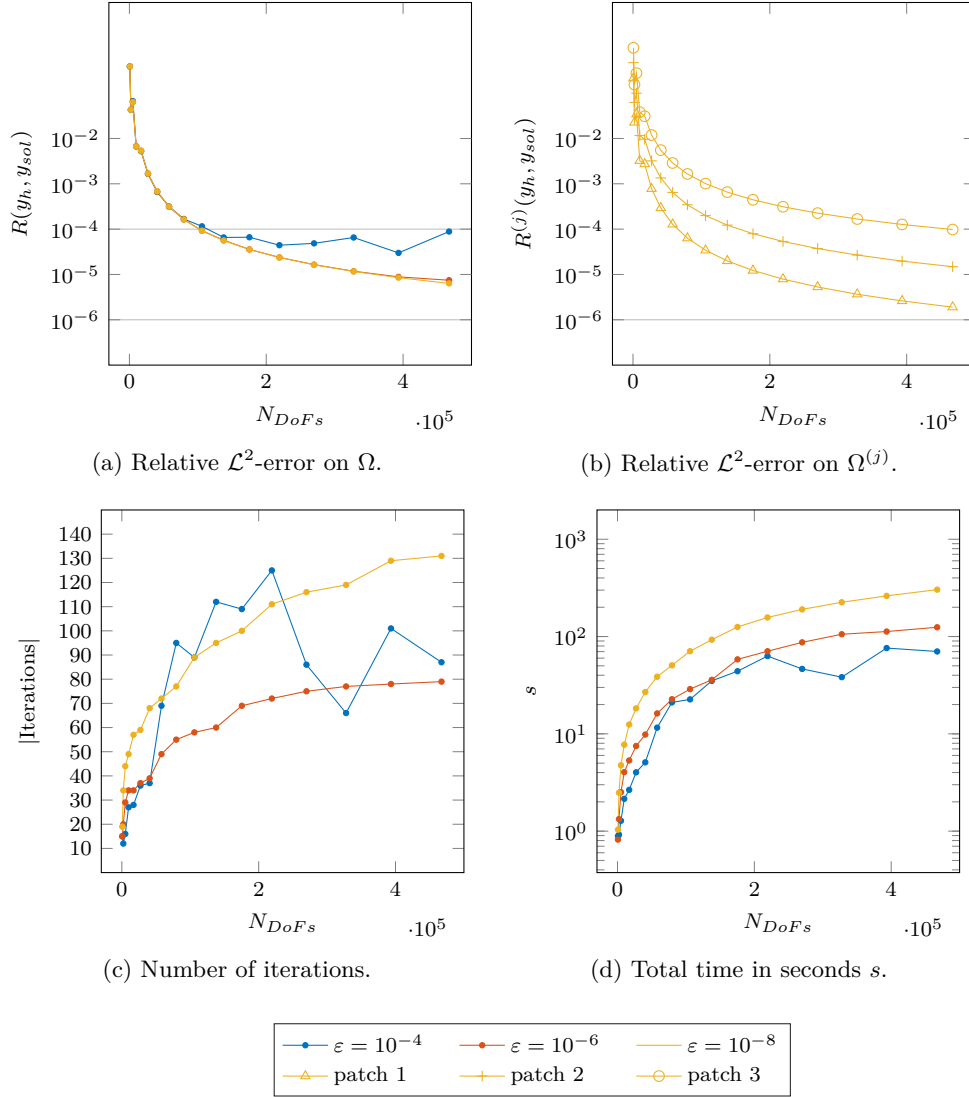


Fig. 4: Performance for different refinements and tolerances on the nonconforming multi-patch geometry with 4 cuboids shown in 3a with (6.3) as analytical solution.

i.e. for solving (4.2) we use `tt_gmres_block.m`² and for solving the local linear systems inside (4.2) we use `amen_solve2.m`³. As before we use `amen_block_solve.m` for solving the weight function interpolation system (2.9) with a tolerance of 10^{-8} .

We show in Figure 7 the results for the multi-patch geometry shown in Figure 3a with desired state defined by (6.5) where $y_{sol}(x, y, z)$ is defined by (6.3). We use B-splines of degree 3 in both the conforming case and the nonconforming case. In the

²with parameters `max_iters` = 10, `restart` = 20 and `tol` = 10^{-6}

³with parameters `nswp` = 20, `kickrank` = 2 and `tol` = 10^{-7}

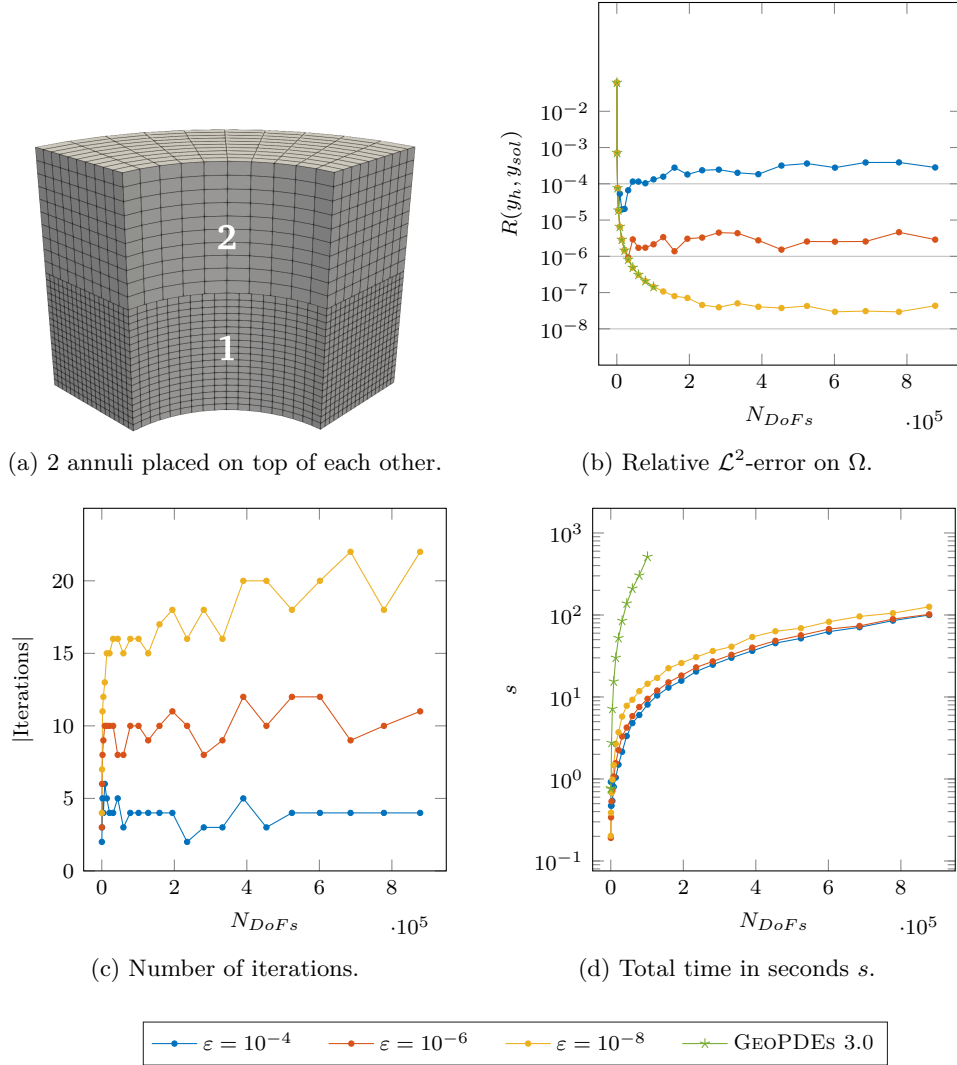


Fig. 5: Performance for different refinements and tolerances on the conforming multi-patch geometry with 2 annuli shown in 5a with (6.4) as analytical solution.

conforming case we have a discretization of $N_{DoFs}^{(j)} = 373.248$ DoFs for $j = 1, \dots, 4$, so that we consider a total of 14.929.920 many DoFs for $N_t = 10$ time steps. In the nonconforming case we have the division $N_{DoFs}^{(1)} = 357.911$, $N_{DoFs}^{(2)} = 50.653$, $N_{DoFs}^{(3)} = 8000$, so that we consider a total of 4.672.170 DoFs with $N_t = 10$. We observe in both cases that the objective function value decreases while the norm of the control increases for decreasing α . The number of iterations is small which suggests that the preconditioner approximates the full operator sufficiently and hence reducing the number of TT-GMRES iterations. The computational times remain moderate in both cases and do only slightly vary in a similar way as the number of iterations, which is to be expected.

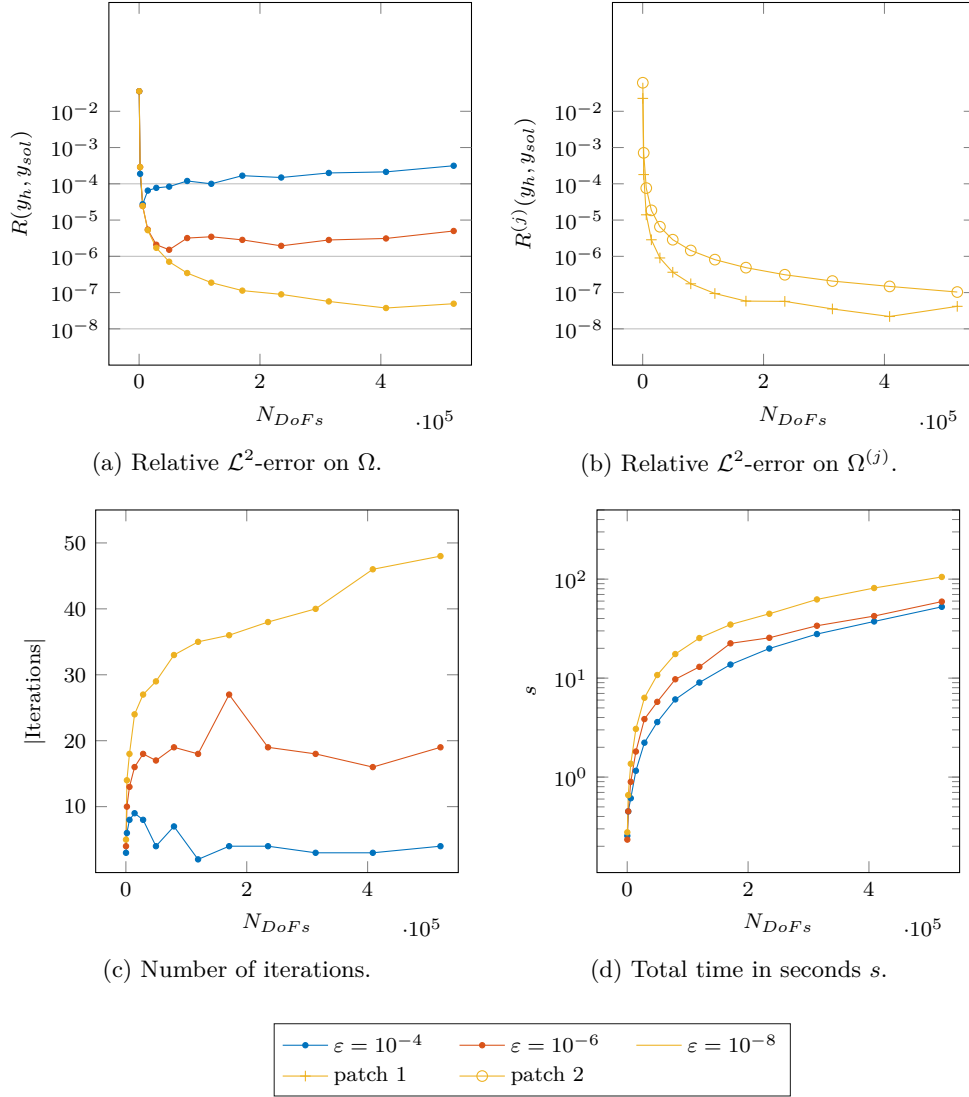


Fig. 6: Performance for different refinements and tolerances on the nonconforming multi-patch geometry with 2 annuli shown in 5a with (6.4) as analytical solution.

We show in Figure 8 the results for the multi-patch geometry shown in Figure 5a with desired state defined by (6.5) where $y_{sol}(x, y, z)$ is defined by (6.4). We use B-splines of degree 3 in both the conforming case and the nonconforming case. In the conforming case we have a discretization of $N_{DoFs}^{(j)} = 438.976$ DoFs for $j = 1, 2$, so that we consider a total of 8.779.520 many DoFs for $N_t = 10$ time steps. In the nonconforming case we have the division $N_{DoFs}^{(1)} = 456.533$, $N_{DoFs}^{(2)} = 64.000$, so that we consider a total of 5.205.330 DoFs with $N_t = 10$. We observe similar results here.

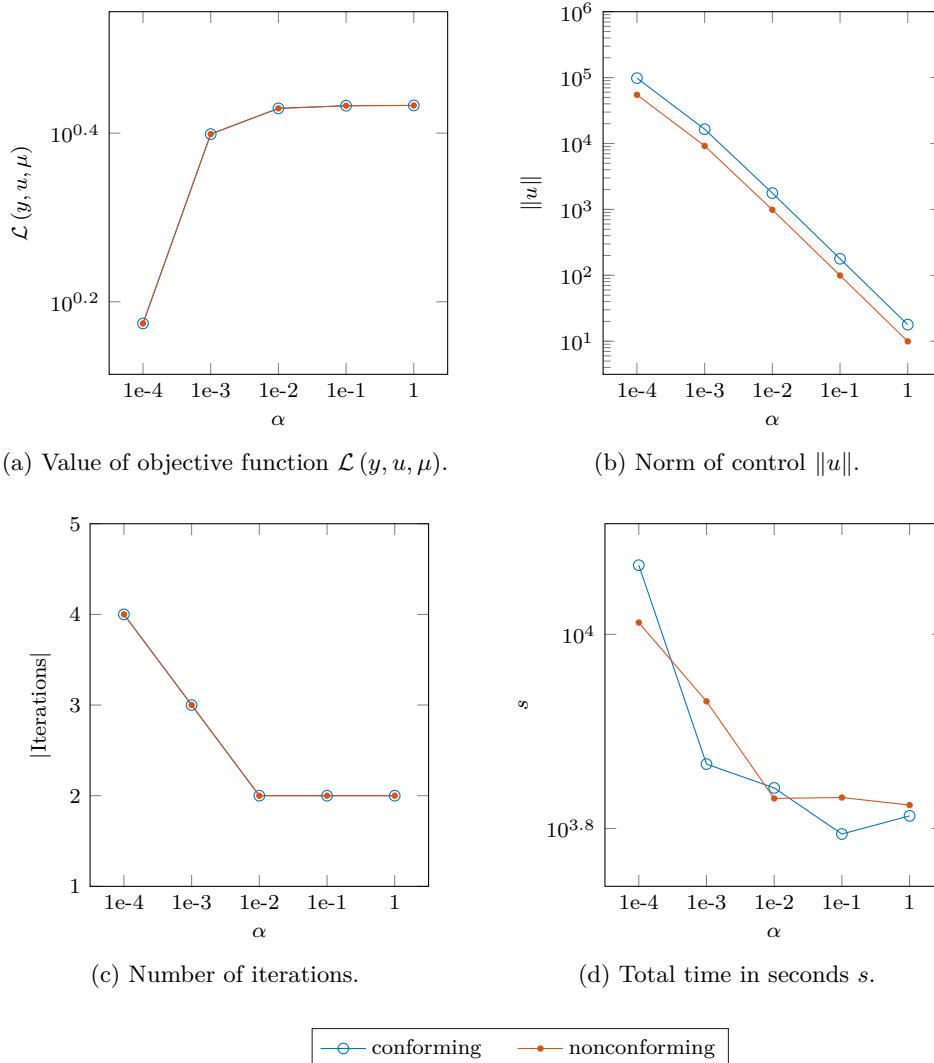


Fig. 7: Stability of the method presented in section 5 depending on the parameter α on the multi-patch geometry with 4 cuboids shown in 3a for the conforming and not nonconforming case.

7. Conclusion. In this paper, we transferred the TT low-rank method presented by Bünger et al. [5] to the multi-patch setting using the idea of the IETI method from [15]. The C^0 -continuity of the approximation across the patch interfaces was ensured by defining a jump tensor which can be represented in TT format. The resulting linear system is highly structured and we showed that the solution can be approximated using TT-based solvers that rely on special GMRES iteration and the design of efficient but also easy to use preconditioners. We applied the resulting scheme to solve large-scale optimal control problems, where we introduced a preconditioned GMRES method that can deal with differently sized PDE and constraint blocks. We

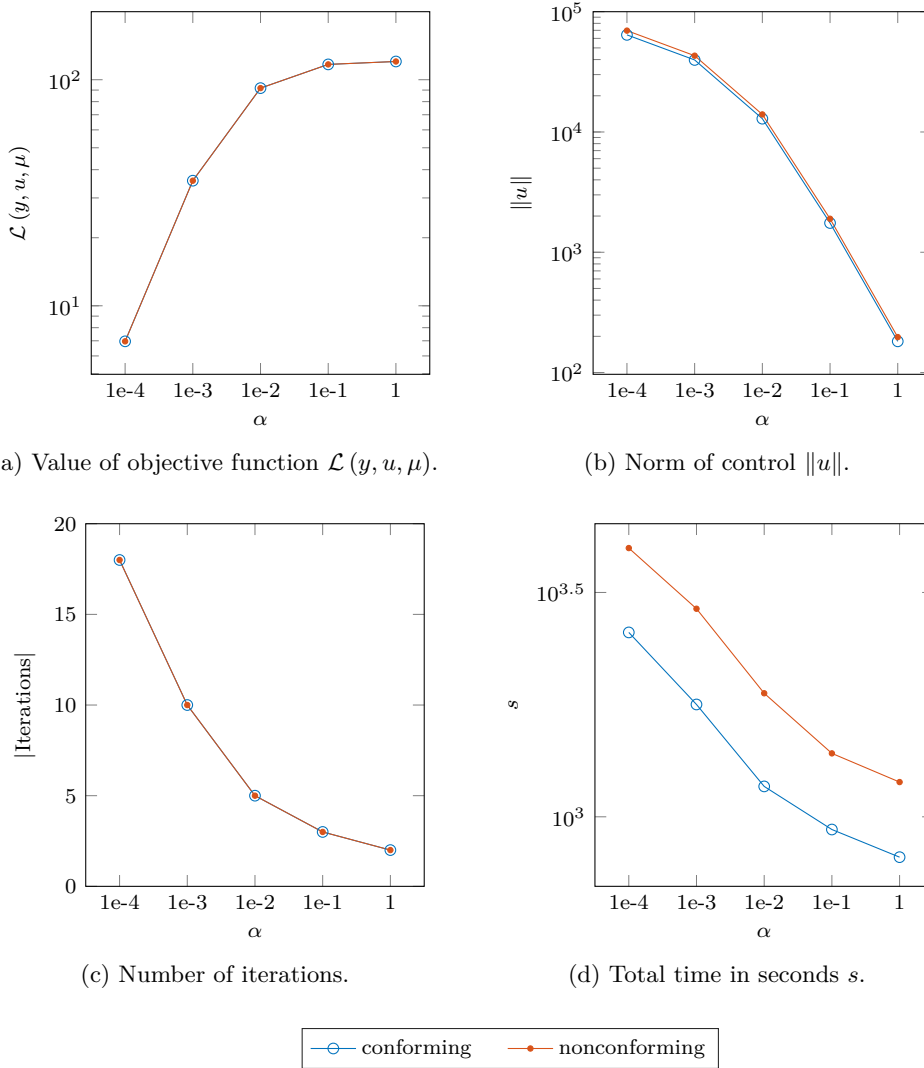


Fig. 8: Stability of the method depending on the parameter α on the multi-patch geometry with 2 annuli shown in 5a for the conforming and not nonconforming case.

also equipped the method with a preconditioner that allowed for a robust performance of our scheme. We then illustrate the performance of our both methods on several multi-patch testcases.

REFERENCES

- [1] P. ANTOLIN, A. BUFFA, F. CALABRÓ, M. MARTINELLI, AND G. SANGALLI, *Efficient matrix computation for tensor-product isogeometric analysis: The use of sum factorization*, *Comput. Method. Appl. M.*, 285 (2015), pp. 817 – 828.
- [2] P. BENNER, S. DOLGOV, A. ONWUNTA, AND M. STOLL, *Low-rank solvers for unsteady Stokes–Brinkman optimal control problem with random data*, *Comput. Method. Appl. M.*, 304

- (2016), pp. 26–54.
- [3] M. BENZI, H. G. GOLUB, AND J. LIESEN, *Numerical solution of saddle point problems*, Acta Numerica, 14 (2005), pp. 1–137.
 - [4] A. BÜNGER, *Low-rank tensor method for isogeometric analysis*, 2020. tu-chemnitz.de/mathematik/wire/codes.php, Accessed: 2024-05-10.
 - [5] A. BÜNGER, S. DOLGOV, AND M. STOLL, *A low-rank tensor method for PDE-constrained optimization with isogeometric analysis*, SIAM Journal on Scientific Computing, 42 (2020), pp. A140–A161.
 - [6] L. DE LATHAUWER, B. DE MOOR, AND J. VANDEWALLE, *A multilinear singular value decomposition*, SIAM Journal on Matrix Analysis and Applications, 21 (2000), pp. 1253–1278.
 - [7] V. DE SILVA AND L.-H. LIM, *Tensor rank and the ill-posedness of the best low-rank approximation problem*, SIAM J. Matrix Anal. Appl., 30 (2008), pp. 1084–1127.
 - [8] S. DOLGOV, *TT-GMRES: Solution to a linear system in the structured tensor format*, Russian Journal of Numerical Analysis and Mathematical Modelling, 28 (2013).
 - [9] S. DOLGOV AND M. STOLL, *Low-rank solution to an optimization problem constrained by the Navier–Stokes equations*, SIAM J. Sci. Comput., 39 (2017), pp. A255–A280.
 - [10] S. V. DOLGOV AND D. V. SAVOSTYANOV, *Alternating minimal energy methods for linear systems in higher dimensions*, SIAM J. Sci. Comput., 36 (2014), pp. A2248–A2271.
 - [11] H. C. ELMAN, D. J. SILVESTER, AND A. J. WATHEN, *Finite elements and fast iterative solvers: with applications in incompressible fluid dynamics*, Numerical Mathematics and Scientific Computation, Oxford University Press, Oxford, second ed., 2014.
 - [12] R. HERZOG AND O. RHEINBACH, *FETI-DP methods for optimal control problems*, Lecture Notes in Computational Science and Engineering, 98 (2014), pp. 387–395.
 - [13] T. HUGHES, J. COTTRELL, AND Y. BAZILEVS, *Isogeometric analysis: CAD, finite elements, NURBS, exact geometry and mesh refinement*, Comp. Methods Appl. Mech. Eng., 194 (2005), pp. 4135–4195.
 - [14] T. HUGHES, A. REALI, AND G. SANGALLI, *Efficient quadrature for NURBS-based isogeometric analysis*, Comp. Methods Appl. Mech. Eng., 199 (2010), pp. 301 – 313.
 - [15] S. KLEISS, C. PECHSTEIN, B. JÜTTLER, AND S. TOMAR, *IETI – Isogeometric Tearing and Interconnecting*, Computer Methods in Applied Mechanics and Engineering, 247-248 (2012), pp. 201–215.
 - [16] A. MANTZAFARIS, B. JÜTTLER, B. N. KHOROMSKIJ, AND U. LANGER, *Matrix generation in isogeometric analysis by low rank tensor approximation*, in Curves and Surfaces: 8th International Conference, Paris, France, June 12-18, 2014, Revised Selected Papers, Springer International Publishing, 2015, pp. 321–340.
 - [17] ———, *Low rank tensor methods in Galerkin-based isogeometric analysis*, Comp. Methods Appl. Mech. Eng., 316 (2017), pp. 1062–1085.
 - [18] A. MANTZAFARIS, F. SCHOLZ, AND I. TOULOPOULOS, *Low-rank space-time decoupled isogeometric analysis for parabolic problems with varying coefficients*, Comp. Methods Appl. M., (2018 in press).
 - [19] M. MONTARDINI, G. SANGALLI, AND M. TANI, *A low-rank isogeometric solver based on Tucker tensors*, Computer Methods in Applied Mechanics and Engineering, 417 (2023), p. 116472.
 - [20] M. MONTARDINI, G. SANGALLI, AND M. TANI, *A low-rank solver for conforming multipatch isogeometric analysis*, 2024.
 - [21] V. P. NGUYEN, C. ANITESCU, S. P. BORDAS, AND T. RABCZUK, *Isogeometric analysis: an overview and computer implementation aspects*, Mathematics and Computers in Simulation, 117 (2015), pp. 89–116.
 - [22] I. OSELEDETS, *Tensor-train decomposition*, SIAM J. Scientific Computing, 33 (2011), pp. 2295–2317.
 - [23] I. V. OSELEDETS, *Tensor-train decomposition*, SIAM J. Sci. Comput., 33 (2011), pp. 2295–2317.
 - [24] I. V. OSELEDETS, S. DOLGOV, V. KAZEEV, D. SAVOSTYANOV, O. LEBEDEVA, P. ZHLOBICH, T. MACH, AND L. SONG, *TT-Toolbox*, 2011. <https://github.com/oseledets/TT-Toolbox>.
 - [25] I. V. OSELEDETS AND S. V. DOLGOV, *Solution of linear systems and matrix inversion in the TT-format*, SIAM J. Sci. Comput., 34 (2012), pp. A2718–A2739.
 - [26] M. PAN, B. JÜTTLER, AND A. GIUST, *Fast formation of isogeometric Galerkin matrices via integration by interpolation and look-up*, Computer Methods in Applied Mechanics and Engineering, 366 (2020), p. 113005.
 - [27] M. PAN, B. JÜTTLER, AND A. MANTZAFARIS, *Efficient matrix assembly in isogeometric analysis with hierarchical B-splines*, Journal of Computational and Applied Mathematics, 390 (2021), p. 113278.
 - [28] J. W. PEARSON, M. STOLL, AND A. J. WATHEN, *Regularization-robust preconditioners for time-dependent PDE-constrained optimization problems*, SIAM J. Matrix Anal. Appl., 33

- (2012), pp. 1126–1152.
- [29] L. PIEGL, *On NURBS, a survey*, IEEE Computer Graphics and Applications, 11 (1991), pp. 55–71.
 - [30] L. PIEGL AND W. TILLER, *The NURBS Book*, Monographs in Visual Communication, Springer Berlin Heidelberg, 1996.
 - [31] M. SORENSEN, D. LATHAUWER, P. COMON, S. ICART, AND L. DENEIRE, *Canonical polyadic decomposition with a columnwise orthonormal factor matrix*, SIAM Journal on Matrix Analysis and Applications, 33 (2012), pp. 1190–1213.
 - [32] D. SPINK, *Nurbs toolbox*.
 - [33] M. STOLL AND T. BREITEN, *A low-rank in time approach to PDE-constrained optimization*, SIAM J. Sci. Comput., 37 (2015), pp. B1–B29.
 - [34] G. STRANG AND G. FIX, *An Analysis of the Finite Element Method*, Wellesley-Cambridge Press, 2008.
 - [35] R. VÁZQUEZ, *A new design for the implementation of isogeometric analysis in Octave and Matlab: GeoPDEs 3.0*, Computers & Mathematics with Applications, 72 (2016), pp. 523–554.